

THE HUNT FOR EXOMOONS WITH KEPLER (HEK):  
V. A SURVEY OF 41 PLANETARY CANDIDATES FOR EXOMOONS <sup>†</sup>

D. M. Kipping<sup>1</sup>, A. R. Schmitt<sup>2</sup>, X. Huang<sup>3</sup>, G. Torres<sup>4</sup>,  
D. Nesvorný<sup>5</sup>, L. A. Buchhave<sup>4,6</sup>, J. Hartman<sup>3</sup>, G. Á. Bakos<sup>3,7,8</sup>

Draft version April 30, 2018

ABSTRACT

We present a survey of 41 *Kepler* Objects of Interest (KOIs) for exomoons using Bayesian photodynamics, more than tripling the number of KOIs surveyed with this technique. We find no compelling evidence for exomoons although thirteen KOIs yield spurious detections driven by instrumental artifacts, stellar activity and/or perturbations from unseen bodies. Regarding the latter, we find seven KOIs exhibiting  $> 5\sigma$  evidence of transit timing variations, including the “mega-Earth” Kepler-10c, likely indicating an additional planet in that system. We exploit the moderately large sample of 57 unique KOIs surveyed to date to infer several useful statistics. For example, although there is a diverse range in sensitivities, we find that we are sensitive to Pluto-Charon mass-ratio systems for  $\simeq 40\%$  of KOIs studied and Earth-Moon mass-ratios for 1 in 8 cases. In terms of absolute mass, our limits probe down to 1.7 Ganymede masses, with a sensitivity to Earth-mass moons for 1 in 3 cases studied and to the smallest moons capable of sustaining an Earth-like atmosphere ( $0.3 M_{\oplus}$ ) for 1 in 4. Despite the lack of positive detections to date, we caution against drawing conclusions yet, since our most interesting objects remain under analysis. Finally, we point out that had we searched for the photometric transit signals of exomoons alone, rather than using photodynamics, we estimate that 1 in 4 KOIs would have erroneously been concluded to harbor exomoons due to residual time correlated noise in the *Kepler* data, posing a serious problem for alternative methods.

*Subject headings:* techniques: photometric — planetary systems

1. INTRODUCTION

The occurrence rate, and even the existence, of moons orbiting extrasolar planets is presently unknown. Their discovery would provide, for the first time, information on the physical processes governing satellite formation and evolution outside the Solar System. Additionally, even null detections can guide theory in this respect, when carefully interpreted in terms of upper limits using the appropriate statistical techniques. Since it is a-priori unknown whether exomoons are sufficiently large to be detected using current instrumentation, this realization motivates a survey program to be designed such that statistically rigorous upper limits are derived for null detections. Whilst this strategy necessitates substantially greater computational resources, a survey adopting this philosophy has a guaranteed science product even if no confirmed objects are ever found, which in this case is the occurrence of exomoons as a function of the planet and satellite properties.

The “*Hunt for Exomoons with Kepler*” (HEK) project

(Kipping et al. 2012) is a survey for exomoons around transiting exoplanets which follows this ethos. Our survey uses Bayesian inference to derive rigorous upper limits in the cases of null detections and employs a suite of vetting strategies to interrogate candidate signals, honed by our past experience of conducting this survey. In previous works, we surveyed 18 *Kepler* Objects of Interest (KOIs) for evidence of exomoons including a sample of M-dwarf host stars (Kipping et al. 2014a), habitable-zone KOIs (Kipping et al. 2013b), dynamically active systems (Nesvorný et al. 2012) and single KOIs (Kipping et al. 2013a). In each case, we searched for both the transits of the exomoon and the perturbations induced by its mass with a self-consistent, analytic, dynamical model known as LUNA (Kipping 2011). Correlated noise structure is a particularly frequent source of exomoon transit false-positives, as outlined in the cautionary tale of Kepler-90g.01 (Kipping et al. 2015).

In this paper, we dramatically increase the number of planetary candidates surveyed by HEK, presenting an analysis of 41 KOIs. Since two of these were already studied by previous surveys (but with fewer data), this paper brings the total number of unique KOIs surveyed for exomoons by HEK to 57. The paper is split as follows. In §2, we describe our target selection strategy for these 41 KOIs via three distinct pathways. In §3, the data handling, modeling and inference methods are described, including the vetting and classification strategies we employ. In §4, we present the results of our survey, including refined planet parameters and an analysis of transit timing variations. We conclude in §5 with a discussion focussed on some statistical results from this sample and the HEK surveys to date, including empirical

<sup>1</sup> Dept. of Astronomy, Columbia University, 550 W 120th St., New York, NY 10027, USA; email: dkippling@astro.columbia.edu

<sup>2</sup> Citizen Science

<sup>3</sup> Dept. of Astrophysical Sciences, Princeton University, Princeton, NJ 05844, USA

<sup>4</sup> Harvard-Smithsonian Center for Astrophysics, Cambridge, MA 02138, USA; email: dkippling@astro.columbia.edu

<sup>5</sup> Dept. of Space Studies, Southwest Research Institute, 1050 Walnut St., Suite 300, Boulder, CO 80302, USA

<sup>6</sup> Centre for Star and Planet Formation, Natural History Museum of Denmark, University of Copenhagen, DK-1350 Copenhagen, Denmark

<sup>7</sup> Alfred P. Sloan Fellow

<sup>8</sup> Packard Fellow

<sup>†</sup> Based on archival data of the *Kepler* telescope.

sensitivity limits and computational demands.

## 2. TARGET SELECTION

### 2.1. Overview

As outlined in Kipping et al. (2012), the HEK project utilizes three complementary methods of selecting targets for analysis:

- **TSA:** Target Selection Automatic
- **TSV:** Target Selection Visual
- **TSO:** Target Selection via Opportunities

In previous papers, we limited our samples to targets selected using just one of these methods. In this work, thanks to the larger number of KOIs under consideration, we selected multiple targets from each category. Specifically, our sample consists of 16 KOIs selected via TSA, 16 via TSV and 9 via TSO, as described below. The full list of KOIs considered here is listed in Table 1.

### 2.2. Target Selection Automatic (TSA)

The TSA algorithm is unchanged from that described in Kipping et al. (2014a) and references therein. In summary, the algorithm assigns an estimated mass and tidal properties (specifically  $k_{2P}/Q$ ) to each KOI based on the size from empirical and theoretical relations. Assuming loss through tidal evolution, we are then able to compute the maximum moon mass that can survive for 5 Gyr using the expressions of Barnes & O’Brien (2002). This maximum moon mass is then converted into a radius using an appropriate mass-radius relation and finally into a signal-to-noise ratio (SNR) using the *Kepler* Combined Differential Photometric Precision (CDPP) statistics (Christiansen et al. 2012).

Target KOIs were selected from the NASA Exoplanet Archive list of KOIs, excluding objects flagged as false-positives. In this work, we elect to restrict the TSA targets to those KOIs with radii  $R_P > 2 R_\oplus$ , insolation  $S_{\text{eff}} < 6.925 S_\oplus$  (inner edge of the habitable-zone defined by Zsom et al. 2013) and  $\text{SNR} > 4/\sqrt{0.75} = 4.62$ . The  $\sqrt{0.75}$  scaling is based on the fact TSA computes SNR assuming one uses the entire time series, but in reality we only use 75% of the data in our fits for reasons described in §3.

In total, 25 targets satisfied these criteria, of which three have already been studied in previous surveys (Kepler-22b, Kipping et al. 2013b; KOI-1596.02, Kipping et al. 2014a; KOI-1876.01, Kipping et al. 2013a). Since significantly more data is now available for KOI-1876.01 than available for the analysis in Kipping et al. (2013a), this target was kept in our TSA sample. KOI-1871.01 and KOI-2762.01 were removed from this subset because they were flagged as candidates by the TSV process described later in §2.3. Additionally, KOI-1174.01, KOI-490.02 and KOI-1274.01 (also known as Kepler-421b; Kipping et al. 2014b) have fewer than three visible transits and were rejected. Finally, KOI-902.01 was reported by Mazeh et al. (2013) to display high-amplitude ( $\gtrsim 100$  mins) and long-period ( $\gtrsim 3$  years) transit timing variations (TTVs), which are uncharacteristic of exomoons (Kipping 2009a), and so was also rejected. This resulted in the 16 KOIs listed in Table 1.

### 2.3. Target Selection Visual (TSV)

In previous HEK papers, the only target picked for analysis using our TSV process was KOI-0872.01, also known as Kepler-46b (see the Supporting Online Material of Nesvorný et al. 2012). This target displayed in-transit flux increases characteristic of star-planet-moon mutual events (as well as large TTVs), but these were ultimately attributed to star-spot crossings (e.g. see Béky et al. 2014) rather than due to an exomoon.

In the earlier work, TSV was conducted using several publicly available light curve viewers. However, we quickly found that these viewers did not meet our needs for performing large scale visual surveys. In a typical survey, four to five thousand KOI transit signals need to be examined for exomoon signals across several hundred distinct planetary candidates. To effectively handle such a large volume of data in a reasonable time frame requires a system with advanced navigation and signal processing features, which the public tools did not provide.

To address these needs, we developed a custom designed software package known as LcTools. This package consists of two main components: LcGenerator for generating normalized light curve files in bulk, and LcViewer for examining light curve files and recording signals. This Windows-based software is freely available and can be obtained from the author (A. Schmitt) upon request. We direct those interested to the online description for technical details<sup>10</sup>, but we briefly point out some relevant features here:

- Bin short-cadence (SC) data to a user specified cadence.
- Independently pan and scale the time and flux axes.
- Locate each instance of a periodic signal and automatically scale the signal for optimized viewing.
- Automatically highlight known transit signals according to the NASA Exoplanet Archive ephemerides (e.g. see Figure 1).
- Automatically highlight mutual planetary transit signals (the simultaneous transit of two or more planets).
- Record and highlight user-defined signals (e.g. due to exomoons), as shown in Figure 1.

In total, 1289 unique KOIs were examined for exomoon signals across numerous surveys. Many KOIs were inspected multiple times. KOIs included both TSAs and non-TSAs. The latter group was largely composed of promising targets meeting the selection criteria below:

- ▶ Semi-major axis;  $a \geq 0.1$  AU (for reasons discussed in Namouni 2010).
- ▶ Planet size;  $R_P \geq 3 R_\oplus$ .
- ▶ Expected SNR for an exomoon satisfies  $\text{SNR} \geq 1$ .

In all cases, the minimum transit duration required was four hours. From experience, we find that at least eight

<sup>10</sup> See <http://www.exomoon.org> for details

TABLE 1  
List of KOIs surveyed for exomoons in this work, and their basic parameters taken from the NASA Exoplanet Archive.

KOI	$P_P$ [d]	$R_P$ [ $R_\oplus$ ]	SNR	Multip.	$T_{\text{eq}}$ [K]	$T_{\text{eff}}$ [K]	$K_p$	Planet Name	Validation Ref.
<b>16 via TSA</b>									
KOI-0438.02	52.7	2.06	6.77	2	298	3985	14.3	Kepler-155c	Rowe et al. (2014)
KOI-0518.03	247.4	2.14	9.74	3	212	4590	14.3	Kepler-174d	Rowe et al. (2014)
KOI-0854.01	56.1	2.05	5.73	1	252	3593	15.8	-	-
KOI-0868.01	236.0	8.73	7.13	1	172	3822	11.6	-	-
KOI-1361.01	59.9	2.53	7.38	1	298	4014	15.0	Kepler-61b	Ballard et al. (2013)
KOI-1431.01	345.2	8.00	4.65	1	272	5628	13.5	-	-
KOI-1783.02	284.0	4.80	4.79	2	321	6215	13.9	-	-
KOI-1830.02	198.7	2.88	6.03	2	257	5080	14.4	-	-
KOI-1876.01	82.5	2.56	7.78	1	276	4237	15.2	-	-
KOI-2020.01	111.0	2.32	10.17	1	260	4441	15.5	-	-
KOI-2686.01	211.0	3.68	7.21	1	233	4628	13.9	-	-
KOI-2691.01	97.5	3.30	6.35	1	313	4728	15.0	-	-
KOI-3263.01	76.9	7.00	5.03	1	211	3587	15.9	-	-
KOI-4005.01	178.1	2.22	5.55	1	316	5592	14.6	Kepler-439b	Torres et al. (2015)
KOI-4036.01	168.8	2.24	5.93	1	279	4893	14.1	-	-
KOI-4054.01	169.1	2.21	5.58	1	308	5380	14.6	-	-
<b>16 via TSV</b>									
KOI-0092.01	65.7	3.07	8.70	1	503	5952	11.7	-	-
KOI-0112.01	51.1	3.04	6.74	2	552	5803	12.8	-	-
KOI-0209.01	50.8	9.16	5.29	2	636	6466	14.3	Kepler-117b	Rowe et al. (2014)
KOI-0276.01	41.7	2.71	5.86	1	629	5982	11.9	-	-
KOI-0308.01	35.6	2.88	2.28	1	672	6210	12.4	-	-
KOI-0374.01	172.7	3.14	9.26	1	389	5839	12.2	-	-
KOI-0398.01	51.8	8.77	2.98	3	459	5271	15.3	-	-
KOI-0458.01	53.7	8.16	2.65	1	558	5833	14.7	-	-
KOI-0847.01	80.9	4.83	1.13	1	413	5665	15.2	-	-
KOI-1535.01	70.7	2.13	7.67	1	539	6174	13.0	-	-
KOI-1726.01	45.0	2.01	9.63	1	405	4684	13.1	-	-
KOI-1808.01	89.2	3.82	5.36	1	504	6277	12.5	-	-
KOI-1871.01	92.7	2.25	7.34	2	295	4528	14.9	-	-
KOI-2065.01	80.2	3.60	4.33	1	437	5685	14.3	-	-
KOI-2762.01	133.0	2.15	4.69	1	266	4530	15.0	-	-
KOI-5284.01	389.3	6.79	2.10	1	267	5731	14.6	-	-
<b>9 via TSO</b>									
KOI-0072.02	45.3	2.30	12.44	2	554	5627	11.0	Kepler-10c	Dumusque et al. (2014)
KOI-0245.01	39.8	1.88	49.27	3	456	5417	9.7	Kepler-37d	Barclay et al. (2013)
KOI-0386.02	76.7	2.89	4.15	2	512	6197	13.8	Kepler-146c	Rowe et al. (2014)
KOI-0518.02	44.0	1.43	10.37	3	377	4590	14.3	Kepler-174c	Rowe et al. (2014)
KOI-0722.01	46.4	2.85	3.12	1	635	6343	13.5	-	-
KOI-1783.01	134.5	7.93	6.06	2	412	6215	13.9	-	-
KOI-2358.01	56.5	2.04	6.39	1	583	6412	13.5	-	-
KOI-3663.01	282.5	11.28	5.20	1	328	6007	12.6	PH-2b	Wang et al. (2013)
KOI-3681.01	217.8	22.02	2.58	2	497	6382	11.7	-	-

long-cadence (LC) data points are necessary to reliably detect exomoon signals visually.

For a given host star, all available Presearch Data Conditioning (PDCSAP) data (Stumpe et al. 2012, Smith et al. 2012) were obtained from the Barbara A. Mikulski Archive for Space Telescopes<sup>11</sup> (MAST). The data were normalized and merged into a single light curve file. Both the LC and SC data were used, with SC given priority. To mitigate the flux scatter and improve signal detection, SC data were binned to a lower data rate - typically 6, 10, or 12 data points per hour.

For each KOI transit signal, a visual search was made for moon-like signals within the marked KOI signal region (see Figure 1 for an example). The KOI signal region is defined as the extended Hill timescale per the equation given in §2.2 of Kipping et al. (2013b). Upon finding a

moon-like signal conforming to the general shape characteristics predicted by LUNA (Kipping 2011), the signal was manually recorded in LcViewer and a screen snapshot taken.

A total of 2928 moon-like signals were recorded; 923 from the TSA group and 2005 from the non-TSA group. From this set, the highest quality signals were visually identified. For the current paper, 16 KOIs were found having at least three high quality exomoon signals (see Table 1). Note that this represents just a fraction of the KOIs with high-quality signals found.

#### 2.4. Target Selection via Opportunities (TSO)

In addition to the 32 KOIs selected using the TSA and TSV methods, we picked 9 KOIs as “targets of opportunity” via TSO. This process is loosely defined as identifying systems for which we have reason to suspect an elevated probability of a successful detection or that the

<sup>11</sup> <https://archive.stsci.edu/kepler>

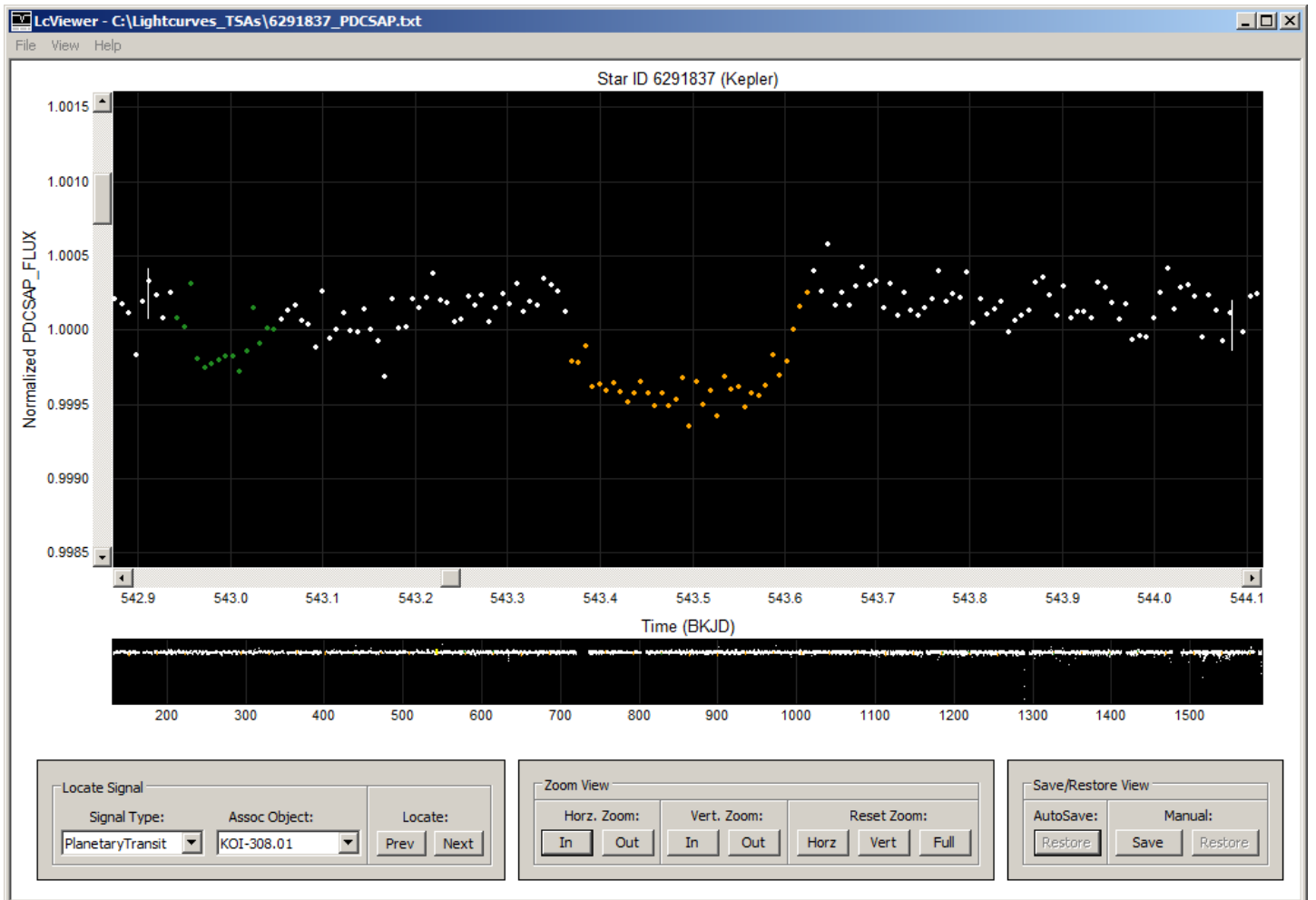


FIG. 1.— Main application window for LcViewer. Two signals are shown in this example: a planetary transit signal of KOI-0308.01 highlighted in orange and a user defined moon-like signal highlighted in green. The white vertical lines on either side of the light curve indicate the region of visual inspection, which is equal to the estimated Hill timescale.

system has some unusual properties making an analysis of greater scientific value. As an example from previous surveys, in Kipping et al. (2013b) we selected Kepler-22b using TSO, since it was claimed to be the first habitable-zone transiting planet discovered (Borucki et al. 2012). Below, we briefly describe the reasons why each KOI was selected using TSO.

KOI-0722.01 was previously surveyed in Kipping et al. (2013a) using quarters Q1-9 of the *Kepler* data, but is re-analyzed here using Q1-17 due to the unusual fits found previously.

KOI-0072.01, also known as Kepler-10c, is a confirmed transiting planet with a mass measured using radial velocities (Dumusque et al. 2014). Argued by the authors to be a solid Neptune-mass planet, Kepler-10c may represent a scaled up version of the Earth leading us to wonder if there is a scaled up version of the Moon in orbit too.

KOI-3663.01, also known as PH-2b, is a validated transiting planet (Wang et al. 2013) found by the Planet Hunters project (Fischer et al. 2012). The discoverers argue that the planet is a Jupiter-sized planet in the habitable-zone of its host star, making it an ideal target for an exomoon search.

KOI-1783.01 and KOI-0518.02 (also known as Kepler-

174c; Rowe et al. 2014) are additional KOIs to two targets already selected in the TSA part of this work, namely KOI-1783.02 and KOI-0518.03 (also known as Kepler-174d; Rowe et al. 2014). Moreover, both of these have relatively high SNR expected due to putative exomoons and so were selected via TSO.

KOI-0245.01, also known as Kepler-37d, is a validated transiting planet and the largest and widest orbit planet in a three-planet system (Barclay et al. 2013). The photometric precision achieved for Kepler-37 is exceptional, thanks to the star’s brightness (9.7 in *Kepler*’s bandpass) and low intrinsic noise, allowing for the discovery of the Moon-sized planet Kepler-37b. For this reason, we added this target through TSO.

KOI-3681.01 was surveyed for exomoons in an independent study (Lewis 2014), but only using the transit method rather than the full photodynamic modeling employed by HEK. Nevertheless, we added this target to exploit the unique opportunity to compare our results.

Finally, KOI-0386.02 and KOI-2358.01 were selected as somewhat “wildcard” targets due to their moderate orbital periods providing plenty of transits (76.7 d and 56.5 d respectively) and yet TSA still predicting reasonably good SNR values of 4.15 and 6.39 respectively.



### 3. ANALYSIS METHODOLOGY

#### 3.1. Data Handling

Photometric time series for the 41 KOIs studied in this work were obtained from the MAST archive. We downloaded all available quarters from Q0-17 for each KOI and preferentially use the SC over LC data, where available. Only data with SAP QUALITY values equal to zero were utilized in this work, thereby rejecting data likely corrupted by known effects.

As with previous papers, we only use the Simple Aperture Photometry (SAP) processed data in our analysis, rather than the Presearch Data Conditioning (PDCSAP) time series (Stumpe et al. 2012, Smith et al. 2012). The PDCSAP data is optimized to remove common mode instrumental effects in order to retain stellar astrophysics such as rotational modulations. However, in our work, retaining the stellar astrophysics is not required and critically the act of cleaning common modes will remove frequencies across the Fourier domain that may potentially distort, remove or even spuriously introduce the very low amplitude exomoon-like signals we seek here.

Transit light curves are detrended on an epoch-by-epoch basis. Transits are initially located using the NASA Exoplanet Archive reported ephemeris and we consider a window of  $\pm 0.5P$  around each event. Discontinuities in the time series, due to pointing tweaks for example, are visually identified and in such cases our epoch window is shortened up to the nearest such event surrounding each transit i.e. we make no attempt to correct such effects. Long-term trends, due to focus drift for example, are removed using the CoFiAM algorithm described in Kipping et al. (2013a, 2014a). This algorithm is essentially a low-cut, high-pass filter removing all long-term trends with a threshold frequency set to three times the NASA Exoplanet Archive reported transit duration. As described in our previous papers, CoFiAM ensures the transit light curve of the planet and any moons are not distorted, whilst removing long-term trends and minimizing the autocorrelation on a 30 minute timescale. It is important to stress that CoFiAM does not remove high frequency noise, but our philosophy here is that whilst one can consider alternative methods to accomplish this feat, it is unclear whether such methods can retain the guarantee of CoFiAM that the transit shape is undisturbed.

#### 3.2. Forward Modeling

As with previous HEK papers, the forward model that is compared to the observations is the LUNA algorithm, described in Kipping (2011). At every time stamp, LUNA calculates the sky-projected positions of the planet and moon relative to the star, using a nested Keplerian body appropriate for a hierarchical three-body problem (see Appendix of Kipping 2010b for proof). Based on these positions, the amount of star light blocked by the planet and the moon are calculated analytically using the Fewell (2006) and Kipping (2011) solutions. Limb darkening of the star is appropriately accounted for, provided the radius of the satellite is small relative to the star i.e.  $R_S \ll R_*$  (this is not required for the planet). In this work, we use the quadratic limb darkening formulation described in Kipping (2013) and account for long-cadence smearing using the re-sampling treatment described in Kipping (2010a) ( $N_{\text{resam}} = 30$ ). Quarter-to-

quarter contaminating light factors are taken from the fits file (“CROWDSAP” header keyword) and accounted for following the method described in Kipping & Tinetti (2010).

Recently, there have been several proposals for finding exomoons using alternative methods to photodynamics, such as excess noise around transits (“scatter-peak”; Simon et al. 2012), high frequency TTVs (Szabó et al. 2013) and phase-stacking transits (“OSE”; Heller et al. 2014), and we briefly comment on why we still favor the photodynamical technique.

The alternative methods aim to be computationally cheaper than photodynamical modeling, at the expense of approximating the complex motions involved. However, it is important to note that photodynamical modeling accounts for all known photometric effects caused by a transiting exomoon, e.g., TTV (Sartoretti & Schneider 1999), TDV-V (Kipping 2009a), TDV-TIP (Kipping 2009b), plus even previously unknown effects such as ingress/egress asymmetries (Kipping 2011). Therefore, these simpler methods can all be understood to be approximations to the full photodynamical description and by definition model less of the information content imparted into the light curve by the presence of exomoon(s). With less information, they are all guaranteed to not only be less sensitive in terms of signal-to-noise, but also critically lacking the powerful vetting techniques available with photodynamics, such as dynamical weighing of the parent planet (Kipping 2010b). We also stress that our implementation of photodynamics models the entire *Kepler* time series, i.e. every transit is modeled simultaneously and self-consistently. Naturally then, there is no more signal-to-noise to be gained by phase-folding or binning techniques (e.g. Simon et al. 2012; Heller et al. 2014), which will actually only serve to further degrade the information content. For these reasons, we argue that photodynamics remains the most robust method of searching for exomoons.

However, the alternative methods are typically much faster and may be useful for identifying interesting systems worthy of more detailed analysis with photodynamics i.e. as a prioritization tool. The HEK project currently adopts this position in its application of the Target Selection Visual process discussed in §2.3.

#### 3.3. Bayesian Inference & Model Selection

For reasons discussed in §1, the HEK project places great importance on the use of rigorous statistical inference techniques in our survey. There are several unique needs of an exomoon survey that shape our choice of methodology:

- The parameter space is complex, highly multi-modal and features curved degeneracies, posing a major challenge to many conventional regression techniques.
- In order to derive an upper limit on the satellite-to-planet mass ratio, ( $M_S/M_P$ ), one must marginalize over the other parameters, such as the moon’s semi-major axis and the three-dimensional architecture of the orbits.
- A planet+moon model has significantly greater freedom than a planet-only case guaranteeing a

higher maximum likelihood, thereby necessitating the use of Bayesian model selection.

It should be recognized that satisfying these needs cannot be accomplished without high computational cost. One of the most efficient algorithms that satisfies these requirements is MULTINEST (Feroz et al. 2008, 2009), based on nested sampling (Skilling 2004), and this is the method employed in this work and in our previous HEK papers. Using MULTINEST, multiple objects (in our case multiple exomoons) are identifiable as separate modes (Feroz et al. 2008, 2013), unless the moons strongly interact. This important feature, utilized since the inaugural HEK paper (Kipping et al. 2012), refutes the claim made in Heller et al. (2014) that OSE is the first method permitting the characterization of multiple moon systems.

For each KOI, we regress at least two models, or hypotheses, to the data. The null hypothesis is  $\mathcal{H}_P$ , a planet-only case (forward model is that of Mandel & Agol 2002), which is compared to the planet+satellite hypothesis,  $\mathcal{H}_S$  (forward model is LUNA). The parameterization of these models is the same as that described in Kipping et al. (2014a) and the priors adopted are listed in Table 2. For both models, a Gaussian likelihood function is adopted in our fits and exomoons are assumed to have near-circular orbits.

As in our previous paper Kipping et al. (2014a), we also have latent priors on the derived mean planetary and satellite densities,  $\rho_P$  and  $\rho_S$  (see Kipping 2010b for how these may be calculated). Specifically, we impose a maximum density for both of  $27.9 \text{ g cm}^{-3}$  (see Kipping et al. 2012 for justification) and a minimum density for  $\rho_P$  of  $0.08 \text{ g cm}^{-3}$  (no such minimum is imposed on  $\rho_S$  to allow null detections of  $M_S/M_P$ ). The purpose of these latent priors is to restrict MULTINEST to only the physically plausible range of solutions (thereby imposing detection criteria B3 automatically; see §3.4). One drawback of this decision is that a zero-radius moon (i.e. a null detection of a moon signal) is forbidden, since  $\rho_S \rightarrow \infty$ . In future surveys, we will likely remove these latent priors to allow us to define upper limits on  $(R_S/R_P)$  as well as the usual  $(M_S/M_P)$ .

Although the photometry has been detrended and normalized using CoFIAM, we allow the out-of-transit baseline flux to be varied in our fits too. This term is linear with respect to the transit model and thus can be minimized analytically at each Monte Carlo realization, which we implement here following the technique described in Kundurthy et al. (2011).

### 3.4. Vetting

For each KOI studied, we obtain the Bayesian evidence and parameter posterior distributions for the planet-only model,  $\mathcal{H}_P$ , and also the planet-with-moon model,  $\mathcal{H}_S$ . This information must be used to assess whether the KOI in question can be claimed to exhibit compelling evidence for the presence of one or more exomoons. In Kipping et al. (2013a), we first defined a list of standardized basic criteria that we use to make this assessment:

- B1** Improved evidence of the planet-with-moon fits at  $\geq 4\sigma$  confidence.
- B2** Planet-with-moon Bayesian evidences indicate both a mass and radius preference for the satellite.

TABLE 2

Priors adopted for the planet and moon parameters in our fits.

Parameter	Prior <sup>†</sup>
<i>Planet Parameters</i>	
$p$	$\mathcal{U}\{0, 1\}$
$\log_{10}(\rho_* [\text{g cm}^{-3}])$	$\mathcal{U}\{-3, 3\}$
$b$	$\mathcal{U}\{0, 2\}$
$P$ [days]	$\mathcal{U}\{\hat{P} - 1, \hat{P} + 1\}^*$
$\tau$ [days]	$\mathcal{U}\{\hat{\tau} - 1, \hat{\tau} + 1\}^*$
$q_1^\times$	$\mathcal{U}\{0, 1\}$
$q_2^\times$	$\mathcal{U}\{0, 1\}$
<i>Moon Parameters</i>	
$(R_S/R_P)$	$\mathcal{U}\{-1, 1\}$
$(M_S/M_P)$	$\mathcal{U}\{0, 1\}$
$a_{SP}$	$\mathcal{U}\{2, 7.897\hat{P}^{2/3}\}^*$
$\cos i_S^\diamond$	$\mathcal{U}\{-1, 3\}$
$\Omega_S$ [rads]	$\mathcal{U}\{-\pi, \pi\}$
$P_S$ [days]	$\mathcal{J}\{0.052, \hat{P}/\sqrt{3}\}^*$
$\phi_S$ [rads]	$\mathcal{U}\{0, 2\pi\}$

<sup>†</sup>  $\mathcal{U}$  and  $\mathcal{J}$  denote a uniform and Jeffrey’s prior

\*  $\hat{P}$  and  $\hat{\tau}$  are the reported ephemeris parameters taken from the NASA Exoplanet Archive

$\times$  Defined in Kipping (2013)

$\diamond$  Defined in Kipping et al. (2013b)

**B3** Parameter posteriors are physical.

**B4** Mass and radius of the moon converge away from zero.

As discussed in §3.3, criterion B3 is enforced for all fits by virtue of our latent priors. This forces the mean density of the planet and the satellite to be within the extreme range discussed in Kipping et al. (2012). It is therefore not explicitly tested. Criterion B1 remains unchanged in this work. Although Bayesian model selection is an important prerequisite for claiming a detection, it is insufficient in isolation since we adopt a Gaussian likelihood function to compute the evidences, and real photometry is never perfectly Gaussian.

As of Kipping et al. (2013b), criteria B2 was modified. Formally, B2 requires running two extra photodynamical models in addition to  $\mathcal{H}_S$ , which naturally slows down our survey speed considerably. In Kipping et al. (2013b), we proposed focussing on the radius aspect of B2 alone, which we dub B2a, and testing the condition by allowing  $\mathcal{H}_S$  to explore “negative radius” exomoons. Such signals correspond to inverted transits and we therefore require a positive radius moon as part of our vetting tests. Negative-radius moons have no physical meaning and are most likely indications of time-correlated noise structure.

For criterion B4, the radius test is not useful for vetting when a latent prior exists on  $\rho_S$ , such as done in this work, since zero-radius moons are forbidden. Instead, we focus on the mass component which remains unbiased and dub the criterion B4a.

These modifications lead to the following basic detection criteria:

**B1** Improved evidence of the planet-with-moon fits at  $\geq 4\sigma$  confidence

**B2a** Planet-with-moon evidences indicate a preference

for a positive radius moon (34.13% quantile of  $(R_S/R_P)$  is positive)

**B4a** Mass of the moon converges away from zero (false alarm probability of a zero-mass moon is  $< 5\%$  using the [Lucy & Sweeney 1971](#) test).

Additionally, [Kipping et al. \(2013a\)](#) defined several “follow-up” criteria of which the most powerful is F2: “The predictive power of the moon model is superior (or at least equivalent) to that of a planet-only model”. This test first requires that we only fit  $\sim 75\%$  of the transits in models  $\mathcal{H}_P$  and  $\mathcal{H}_S$ . We then a) extrapolate the maximum a-posteriori realization of the two hypotheses and require  $\mathcal{H}_S$  to yield a better likelihood and b) same as a), except we repeat for  $10^4$  random draws from the posterior distributions of the two hypotheses and require  $\mathcal{H}_S$  to be superior in 95% of the realizations. These respectively define criteria F2a and F2b.

In practice, we only conduct F2b if F2a is first passed, to save resources. In some instances, the limited number of transits available meant we elected to fit 100% of the data, making F2 unavailable as a test. Otherwise, the  $\sim 25\%$  of ignored data is chosen to be near the median of the available LC and SC transits.

F2 is a powerful tool in vetting exomoons but will be passed by KOIs exhibiting high signal-to-noise sinusoidal TTVs, since a moon-like TTV is also a sinusoid ([Kipping 2009a](#)). KOI-0308.01 and KOI-2691.01 both show very strong evidence for TTVs ( $> 17\sigma$ ) and nearly sinusoidal-like behavior, meaning they both passed F2a and F2b. As a more useful test in these two instances, we define the null model to be a finite-mass, zero-radius moon model  $\mathcal{H}_{S,R0}$ . This model is able to reproduce the sinusoidal TTVs but clearly a real exomoon case should be favored over a model negating the moon’s radius.

### 3.5. Classification

Naively, one might expect a KOI to either be classified as a confirmed exomoon or a null result. In practice, experience has revealed that spurious detections are common and are generally unsuitable for deriving upper limits. For this reason, it is necessary to classify null detections (“ND”) versus false-positives (“FP”). In our project, the upper limit we are interested in is the mass-ratio ( $M_S/M_P$ ), since  $(R_S/R_P)$  is known to be both less sensitive and less reliable e.g. see [Kipping et al. \(2013a,b, 2015\)](#). Therefore, we define null detections as being cases where the posterior distribution of  $(M_S/M_P)$  does not converge away from zero. This is equivalent to criterion B4a, providing a quantitative method of classifying null detections.

False-positives can be due to a variety of effects and in many cases we are unable to find an unambiguous explanation (except that we know an exomoon is unlikely to be responsible). These unknown false positives are dubbed “FP-U”. In cases where instrumental effects are thought to be responsible, we dub the case “FP-I”. A recent example of this was discussed in detail for Kepler-90g.01 in [Kipping et al. \(2015\)](#), where a pixel level effect was found to introduce an exomoon false-positive. Finally, if perturbations from another body are likely responsible, we dub the case “FP-P”. These are identified by assessing whether the TTVs

show a significant signal, with  $\geq 4\sigma$  confidence set as our threshold for classification as FP-P.

## 4. RESULTS

### 4.1. Exomoon Survey Results

#### 4.1.1. Overview

Out of the 41 KOIs surveyed in this work, we find no compelling evidence for exomoons. Using our detection criteria discussed in §3.4, we find that only KOI-0072.01 (Kepler-10c) and KOI-3663.01 (PH-2b) pass these standardized tests. However, in both cases we conclude that the moon candidates are false-positives, albeit for differing reasons discussed shortly.

In Table 3, we summarize the results of our survey for each KOI, providing the 68.3% credible intervals for  $(M_S/M_P)$  and  $(R_S/R_P)$  computed from our marginalized posteriors. We also detail which detection criteria were passed/failed and assign a classification (see §3.5) to each object. For some KOIs, two rows are shown due to two distinct modes in the parameter  $(M_S/M_P)$ . In Figure 2, we show the marginalized posterior of  $(M_S/M_P)$  for each KOI (again showing all modes if more than one present).

#### 4.1.2. Kepler-10c

For KOI-0072.02, also known as Kepler-10c, we elected to use all of the *Kepler* data, rather than the usual 75% strategy discussed in §3.4. This is because KOI-0072.02 is rare in providing us access to an additional vetting test. Specifically, a radial velocity solution exists for this object ([Dumusque et al. 2014](#)), allowing us to compare the radial velocity derived planetary density,  $\rho_P$ , to that from our photodynamical fits. We find two modes for KOI-0072.02 for which the first is a clear null detection, failing criterion B4a. The second mode passes all of our basic detection criteria though, and here the  $\rho_P$  test is of great value. The second mode requires  $\rho_P = 17.1^{+2.0}_{-1.3} \text{ g cm}^{-3}$ , which is highly incompatible with the radial velocity measurement of [Dumusque et al. \(2014\)](#) of  $\rho_P = 7.1 \pm 1.0 \text{ g cm}^{-3}$ . This mode is therefore identified as a false-positive. Furthermore, as discussed in §4.2, KOI-0072.01 shows evidence for TTVs at the  $5.0\sigma$  level, meaning that the likely origin of this spurious detection is perturbations (i.e. FP-P). The consequences of TTVs in the Kepler-10 system are discussed in §4.2.

#### 4.1.3. PH-2b

For KOI-3663.01, also known as PH-2b, all of the basic detection criteria are passed but no follow-up tests are possible due to the small number of transit epochs available (just five). Plotting the maximum a-posteriori realization from model  $\mathcal{H}_S$  reveals a solution driven by weak evidence for moon-like transits in the first four transit epochs (see Figure 3). As discussed later in §4.2, TTVs are not favored for this planet, since model  $\mathcal{H}_P$  is preferred over  $\mathcal{H}_{P,TTV}$  at the  $5\sigma$  level. As a result, the reality of the moon candidate rests solely on the reality of these moon-like transits.

The third moon-like transit, present in Q10, occurs almost perfectly in sync with a data gap caused by

TABLE 3  
*Summary of survey results. KOIs with multiple rows denote multiple modes.*

KOI	$(M_S/M_P)^*$	$(R_S/R_P)$	B1	B2a	B4a	F2a	F2b	Classification	Est. $M_S [M_\oplus]$
KOI-0438.02	< 0.96	$-0.735^{+0.028}_{-0.027}$	✓	X	X	N/A	N/A	ND	< 5.07
KOI-0518.03	< 0.91	$+0.48^{+0.27}_{-0.31}$	✓	✓	X	N/A	N/A	ND	< 5.51
KOI-0854.01	< 0.94	$+0.78^{+0.15}_{-1.23}$	X	✓	X	X	-	ND	< 5.33
KOI-0868.01	$0.0142^{+0.0012}_{-0.0010}$	$-0.076^{+0.014}_{-0.012}$	X	X	✓	N/A	N/A	FP-P	-
KOI-1361.01	< 0.87	$+0.66^{+0.18}_{-0.18}$	X	✓	X	X	-	ND	< 5.36
KOI-1431.01	$0.00171^{+0.00024}_{-0.00023}$	$-0.141^{+0.015}_{-0.014}$	✓	X	✓	N/A	N/A	FP-P	-
KOI-1783.02	$0.49^{+0.24}_{-0.16}$	$-0.264^{+0.037}_{-0.037}$	✓	X	✓	N/A	N/A	FP-P	-
KOI-1830.02	< 0.15	$+0.445^{+0.085}_{-0.089}$	X	✓	X	✓	4 X	ND	< 1.14
KOI-1876.01	< 0.047	$-0.547^{+0.057}_{-0.052}$	X	X	X	N/A	N/A	ND	< 0.31
KOI-2020.01	< 0.0019	$-0.540^{+0.055}_{-0.058}$	✓	X	X	X	-	ND	< 0.11
KOI-2686.01	$0.153^{+0.028}_{-0.019}$	$-0.286^{+0.041}_{-0.035}$	✓	X	✓	X	-	FP-P	-
-	$0.68^{+0.17}_{-0.18}$	$-0.266^{+0.050}_{-0.046}$	✓	X	✓	X	-	FP-P	-
KOI-2691.01†	$0.63^{+0.23}_{-0.20}$	$+0.182^{+0.043}_{-0.040}$	X	✓	✓	X	-	FP-P	-
KOI-3263.01	< 0.0020	$-0.073^{+0.017}_{-0.018}$	X	X	X	N/A	N/A	ND	< 0.041
KOI-4005.01	< 0.30	$-0.471^{+0.094}_{-0.079}$	X	X	X	✓	X	ND	< 1.91
KOI-4036.01	< 0.048	$+0.581^{+0.098}_{-0.115}$	X	✓	X	X	-	ND	< 0.26
KOI-4054.01	< 0.069	$-0.713^{+0.085}_{-0.086}$	X	X	X	X	-	ND	< 0.40
KOI-0092.01	$0.168^{+0.075}_{-0.082}$	$+0.307^{+0.066}_{-0.066}$	X	✓	✓	X	-	FP-U	-
-	< 0.017	$-0.217^{+0.037}_{-0.048}$	X	X	X	X	-	ND	< 0.11
KOI-0112.01	< 0.26	$+0.306^{+0.049}_{-0.044}$	X	✓	X	✓	X	ND	< 2.18
KOI-0209.01	< 0.010	$-0.3003^{+0.0075}_{-0.0072}$	✓	X	X	X	-	ND	< 1.12
KOI-0276.01	< 0.65	$-0.26^{+0.64}_{-0.11}$	X	X	X	X	-	ND	< 4.31
KOI-0308.01†	$0.952^{+0.036}_{-0.070}$	$-0.338^{+0.020}_{-0.019}$	X	X	✓	✓	X	FP-P	-
KOI-0374.01	< 0.60	$+0.205^{+0.050}_{-0.039}$	✓	✓	X	X	-	ND	< 5.03
KOI-0398.01	< 0.021	$-0.181^{+0.041}_{-0.038}$	X	X	X	X	-	ND	< 1.47
KOI-0458.01	$0.74^{+0.15}_{-0.20}$	$+0.857^{+0.087}_{-0.120}$	X	✓	✓	X	-	FP-U	-
-	< 0.88	$+0.66^{+0.21}_{-0.23}$	X	✓	X	X	-	ND	< 71.6
KOI-0847.01	< 0.024	$-0.278^{+0.023}_{-0.025}$	✓	X	X	X	-	ND	< 0.062
KOI-1535.01	< 0.012	$-0.469^{+0.049}_{-0.041}$	X	X	X	X	-	ND	< 0.077
KOI-1726.01	< 0.17	$-0.412^{+0.038}_{-0.032}$	X	X	X	X	-	ND	< 0.97
KOI-1808.01	$0.35^{+0.17}_{-0.11}$	$+0.765^{+0.110}_{-0.085}$	✓	✓	✓	X	-	FP-U	-
KOI-1871.01	< 0.92	$-0.550^{+0.083}_{-0.066}$	X	X	X	✓	X	ND	< 5.36
KOI-2065.01	< 0.40	$+0.669^{+0.077}_{-0.070}$	X	✓	X	X	-	ND	< 2.89
KOI-2762.01	< 0.78	$-0.673^{+0.055}_{-0.047}$	X	X	X	X	-	ND	< 5.16
KOI-5284.01	< 0.84	$+0.447^{+0.073}_{-0.075}$	X	✓	X	N/A	N/A	ND	< 2.51
KOI-0072.02	< 0.0025	$+0.313^{+0.016}_{-0.016}$	✓	✓	X	N/A	N/A	ND	< 0.042 <sup>□</sup>
-	$0.123^{+0.043}_{-0.043}$	$+0.423^{+0.036}_{-0.031}$	✓	✓	✓	N/A	N/A	FP-P <sup>◇</sup>	-
KOI-0245.01	< 0.033	$+0.329^{+0.016}_{-0.017}$	✓	✓	X	X	-	ND	< 0.18
KOI-0386.02	< 0.0059	$+0.434^{+0.027}_{-0.030}$	✓	✓	X	X	-	ND	< 0.046
KOI-0518.02	< 0.011	$-0.370^{+0.042}_{-0.035}$	X	X	X	X	-	ND	< 0.046
-	< 0.92	$+0.80^{+0.13}_{-0.24}$	X	✓	X	✓	X	ND	< 4.02
KOI-0722.01	$0.057^{+0.025}_{-0.020}$	$+0.584^{+0.047}_{-0.055}$	X	✓	✓	X	-	FP-U	-
KOI-1783.01	< 0.030	$-0.169^{+0.034}_{-0.029}$	✓	X	X	N/A	N/A	ND	< 1.21
KOI-2358.01	< 0.015	$+0.543^{+0.056}_{-0.054}$	✓	✓	X	X	-	ND	< 0.090
KOI-3663.01	$0.0079^{+0.0035}_{-0.0030}$	$+0.121^{+0.013}_{-0.011}$	✓	✓	✓	N/A	N/A	FP-I	-
KOI-3681.01	< 0.0029	$+0.121^{+0.006}_{-0.231}$	✓	✓	X	N/A	N/A	ND	< 1.84

N/A: Test not available, since all observed transits were used in basic analysis.

\*: The 95.45% quantile is quoted for  $(M_S/M_P)$  if B4a is not passed.

†: Strong evidence for TTVs; null fit was  $\mathcal{H}_{S,R0}$  rather than  $\mathcal{H}_P$

◇: Classified as a false-positive since  $\rho_P$  from moon model is incompatible with independently measured  $\rho_P$

□: Empirical planetary mass available from radial velocities



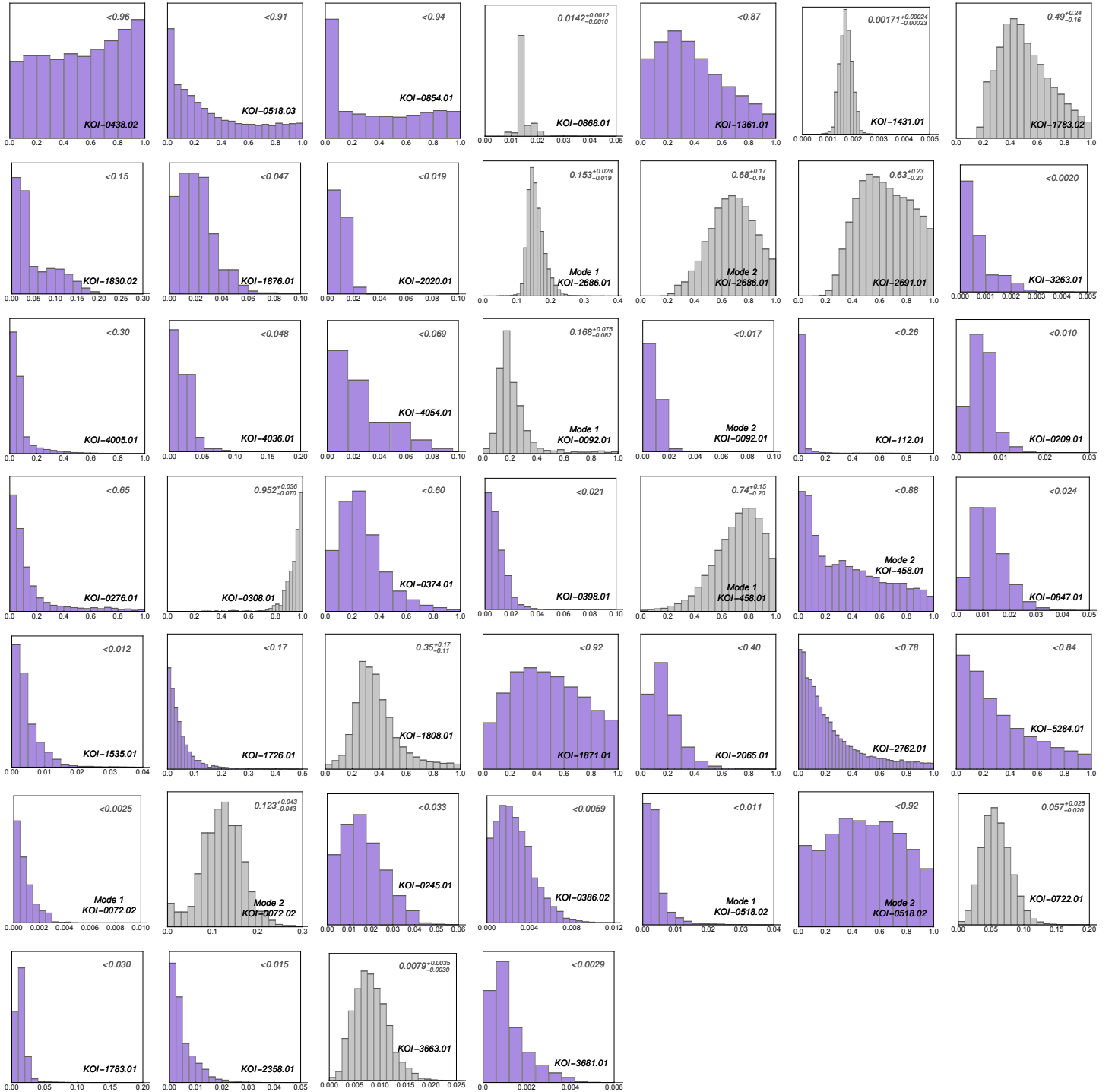


FIG. 2.— Histograms of the parameter ( $M_S/M_P$ ) for the 41 KOIs surveyed in this work. Gray histograms are false-positive exomoons driven by some other perturber, colored ones are null detections. The estimated value of ( $M_S/M_P$ ) is provided in the upper-right corner of each panel.

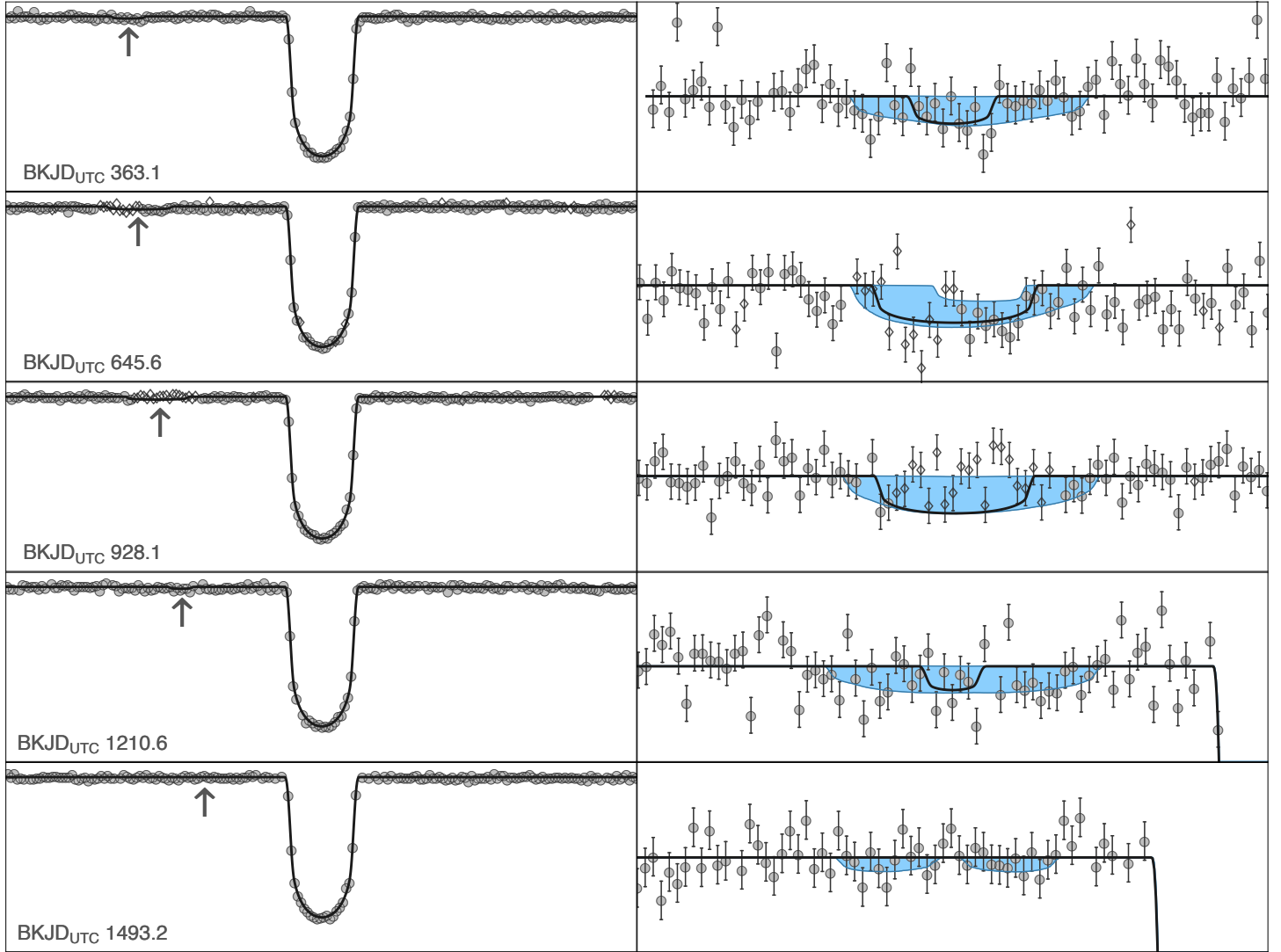


FIG. 3.— Transit light curves of all five epochs (each row) of PH-2b along with the maximum a-posteriori realization from model  $\mathcal{H}_S$  (black line). Right panels show a zoom-in within  $\pm 0.8$  d of the marked point of the left panel. Open diamond data points have zero weight in our fit as they have non-zero SAP QUALITY flags. The blue region denotes the 95.45% confidence interval of our model. The low significance of the model, plus coincidental location of two of the moon signals with instrumental effects, leads to us reject this candidate.

points being ignored by CoFiAM, since the SAP QUALITY flags are non-zero (recall that we do not include such points in our analysis, see §3.1). Specifically, from BKJD<sub>UTC</sub> 926.93 to BKJD<sub>UTC</sub> 927.34, there is a reaction wheel zero crossing. Without these points, there is in fact no data supporting the exomoon transit predicted by model  $\mathcal{H}_S$ . Including the affected data show they are inconsistent with the model, as visible in Figure 3.

For the second moon-like transit there is also a data gap obscuring the expected position of the moon’s ingress signal. Remarkably, as with the aforementioned case, these points were also ignored by CoFiAM due to another reaction wheel zero crossing event. Including the affected points shows that these data are consistent with model  $\mathcal{H}_S$ . However, it should be cautioned that low amplitude non-periodic transit signals, such as this, are known to be reproducible by instrumental artifacts (e.g. see Kipping et al. 2015).

A final blow to the exomoon hypothesis comes from different detrendings of the same time series. For example,

repeating CoFiAM on the PDCSAP data and comparing the maximum a-posteriori model from  $\mathcal{H}_S$  to the PDCSAP detrended data reveals negligible improvement in the  $\chi^2$  versus that of model  $\mathcal{H}_P$ . Specifically, we find  $(\chi_P^2 - \chi_S^2) = +1.7$  for 3560 data points used in our analysis. We repeated this test using a variant of the Trend Filtering Algorithm (TFA) designed for *Kepler* and described in Huang et al. (2013). Here, the results are even worse, with the planet model  $\mathcal{H}_P$  giving a superior explanation of the data with  $(\chi_P^2 - \chi_S^2) = -83.4$ . As a result, we consider this candidate to be an instrumental false-positive, reminiscent of the case of Kepler-90g.01 discussed in Kipping et al. (2015).

## 4.2. Transit Timing Variations

### 4.2.1. Method

We find that 12 of the 41 KOIs surveyed pass criterion B4a, suggestive of a perturbation acting on these objects. To evaluate whether significant TTVs are present for these KOIs, we fit an additional planet model with

freely varied transit times,  $\mathcal{H}_{P,TTV}$ . This model has the same 5 basic shape parameters for usual planets fits (see Table 2) with the global epoch term ( $\tau$ ) and period ( $P$ ) now fixed to the maximum a-posteriori result from model  $\mathcal{H}_P$ . Additionally, for each of the  $N$  transits, an extra free parameter is included for that epoch’s time of transit minimum,  $\tau_i$ , leading to  $(5 + N)$  free parameters. For each KOI, we evaluate the significance of the fit using the usual Bayesian model selection method. The TTVs and the significance of the fit are shown in the right-hand panels of Figure 4. We also compute a periodogram using the method described in Kipping et al. (2013b) (essentially a Lomb-Scargle periodogram with a BIC-based definition of power) and plot the highest power signal over the TTV data.

Since the speed of MULTINEST scales poorly with dimensionality (Handley et al. 2015), we find that KOIs with  $N \geq 17$  were not practical to fit using model  $\mathcal{H}_{P,TTV}$ . Instead, we fit each transit independently fixing the limb darkening coefficients to theoretical values interpolated from the Claret & Bloemen (2011) tabulations and the period,  $P$ , as before, leaving 4 free parameters per fit. We refer to this model as  $\mathcal{H}_{P,I}$  and show the results in Figure 5. Since the summed Bayesian evidence now accounts for excessive freedom, such as duration and depth changes, we instead define a significance for the TTV fit using the Bayesian Information Criterion between the maximum periodogram peak signal and a null fit. These significances are not as statistically robust as the Bayesian evidence method, but serve as a useful proxy.

#### 4.2.2. Dynamically Active KOIs

Seven of twelve systems inspected for TTVs show  $\geq 5\sigma$  evidence for TTVs. Five of these show extremely strong evidence ( $> 17\sigma$ ) for which there can be little doubt the KOIs are being perturbed; specifically KOI-0308.01, KOI-0868.01, KOI-1783.02, KOI-2686.01 and KOI-2691.01. Of these five, only KOI-1783.02 is known to reside in a multiple transiting planet system and the TTV period is compatible with a perturbation from KOI-1783.01, although there is insufficient data to claim so unambiguously. The other four strongly perturbed KOIs are in single KOI systems, indicating at least four additional massive bodies not known to transit the parent star.

Of the two marginal cases for TTVs, KOI-0072.02 and KOI-1431.01, the former is of particular interest being that this is Kepler-10c, the claimed solid Neptune-mass planet measured through radial velocities by Dumusque et al. (2014). Kepler-10b is essentially decoupled from 10c and is not expected to perturb 10c, suggesting an additional unknown massive body in the system. This object is likely to be of planetary mass to have avoided detection by radial velocities thus far. The period and mass of this object cannot be uniquely inferred from a single sinusoidal-like set of TTVs (Nesvorný & Vokrouhlický 2014; Deck & Agol 2014). However, a near mean motion resonance configuration is most probable due to the fact that this configuration leads to the largest amplitude effects. Further, a planet on an exterior orbit would have a greater chance of having not been seen transiting to date, based on the system geometry.

Whilst the evidence for TTVs in Kepler-10c is not de-

cisive, it is worth noting that the radial velocity periodogram (see Dumusque et al. 2014) shows numerous additional peaks to the frequencies of 10b and 10c. Notably, the next largest peak above the 0.1% false alarm probability threshold occurs at 158.54d, almost coincidental with a 7:2 ratio with 10c and potentially responsible for a near mean motion resonance interaction. We recommend additional radial velocities to identify the cause of the observed TTVs.

#### 4.3. Refined Planet Parameters

An additional useful result from this work are parameter posteriors derived for each of the planets surveyed. Since no exomoons are found, we use model  $\mathcal{H}_P$  to estimate refined planetary parameters of each KOI studied. In the cases of the seven dynamically active KOIs, we use the TTV based models instead. The refined parameters are provided in Table 4. Figure 6 illustrates the differences between the parameters derived in this work and those on the NASA Exoplanet Archive, which agree well in general.

## 5. DISCUSSION

### 5.1. Overview

With the 41 KOIs surveyed in this work, the total number of unique KOIs surveyed using Bayesian photodynamics is now 57. In every case, the analysis comes from the HEK project and were reported in Nesvorný et al. (2012) and Kipping et al. (2013a,b, 2014a, 2015). In this survey, as with the previous smaller samples, we find no compelling evidence for an exomoon.

Despite the sizable number of objects surveyed, we caution the community against attempting to derive  $\eta_{\mathcal{C}}$  constraints (the occurrence rate of exomoons) at this time, since some of our most interesting candidates remain under detailed analysis and are yet to be presented. This is an inevitable consequence of the fact that putative candidates require in-depth vetting, such as the case with Kepler-90g.01 where pixel-level analysis was required (Kipping et al. 2015).

### 5.2. Unknown False Positives

Of the 41 KOIs studied, we find four instances of false-positives of unknown origin; KOI-0092.01, KOI-0458.01, KOI-0722.01 and KOI-1808.01. For the first three, criteria B2 and B4a are passed and for KOI-1808.01 all of the basic criteria are satisfied. However, all four KOIs fail the follow-up test, F2a. This means that a Keplerian moon model provides a worse prediction (in a  $\chi^2$  sense) of the  $\sim 25\%$  of ignored transits than a vanilla planet-only model, indicating that a moon cannot explain the observations.

When dealing with a handful of transits, quasi-periodic distortions to the transit profile, such as those due to spots (Béky et al. 2014), can be well fitted by the flexible exomoon model. However, since an exomoon is not the underlying cause, this model lacks any predictive power and thus should fail F2a. We therefore suggest that stellar activity is likely responsible for these four instances. As an example, we briefly discuss the most promising case of KOI-1808.01 which passes all of the basic criteria. Inspection of the posteriors reveals that the planet-moon separation is required to be tight at  $8.2_{-2.2}^{+2.2}$  planetary

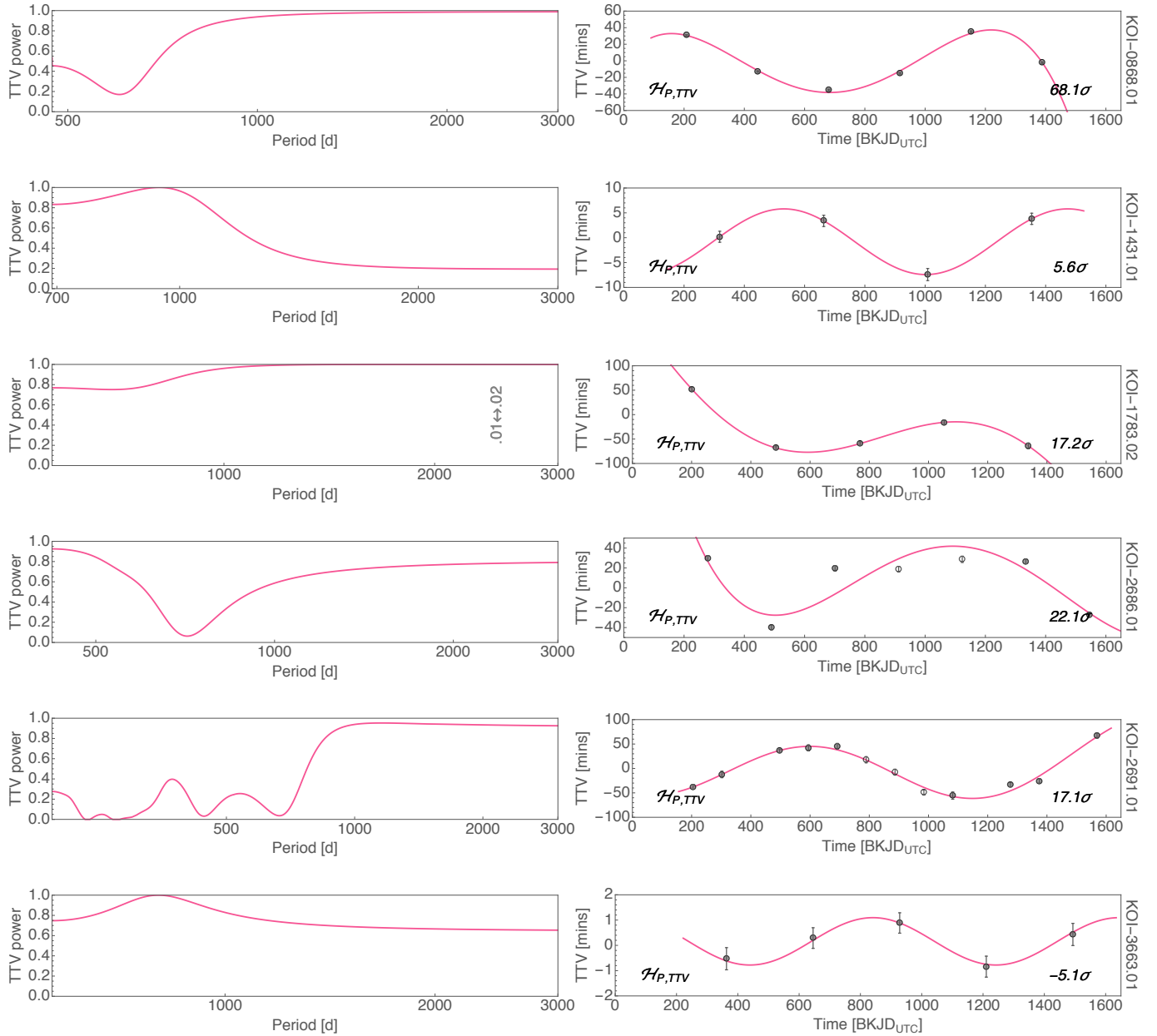


FIG. 4.— Right column shows the TTVs computed for 6 of the 12 KOIs which pass criteria B4a. These 6 KOIs have  $N < 17$  epochs enabling us to conduct the global fit,  $\mathcal{H}_{P,TTV}$ . The left panel shows the corresponding Lomb-Scargle periodogram with a BIC-based definition of power. The favored trial is plotted over the TTV data on the right panel, with the significance denoted in the corner. Negative significances indicate that the TTV model is disfavored.

radii leading to no clean, separated moon transits in the best fit. Instead, the signal is driven by distortions to the planetary transit event, consistent with the effects of spots.

### 5.3. TTV Systems

Although it is not the objective of our work, we find seven systems classed as FP-P, that is exomoon false-positives due to perturbations from another body. These cases display strong evidence for TTVs ( $\geq 5\sigma$ ) and account for 17% of the KOIs surveyed. Curiously, five of these instances occur for the 16 targets selected through TSA, which has a coincidental probability of occurring

of just 7.7%. Since the TSA targets were selected to be in the habitable zone, they are more biased towards long period KOIs, perhaps suggesting that TTVs are more common for such worlds. Whatever the cause, based on the 41 KOIs studied here, habitable zone TSA planetary candidates have an a-priori chance of displaying TTVs of  $(31 \pm 12)\%$ .

This rate is substantially higher than that reported by [Mazeh et al. \(2013\)](#), who find 130 KOIs with significant TTVs out of a total sample of 1897 i.e.  $(6.9 \pm 0.6)\%$ . This is incompatible with the rate seen for the TSAs beyond the inner edge of the habitable zone (as defined by [Zsom et al. 2013](#)) at a level of  $3.2\sigma$ , meaning co-



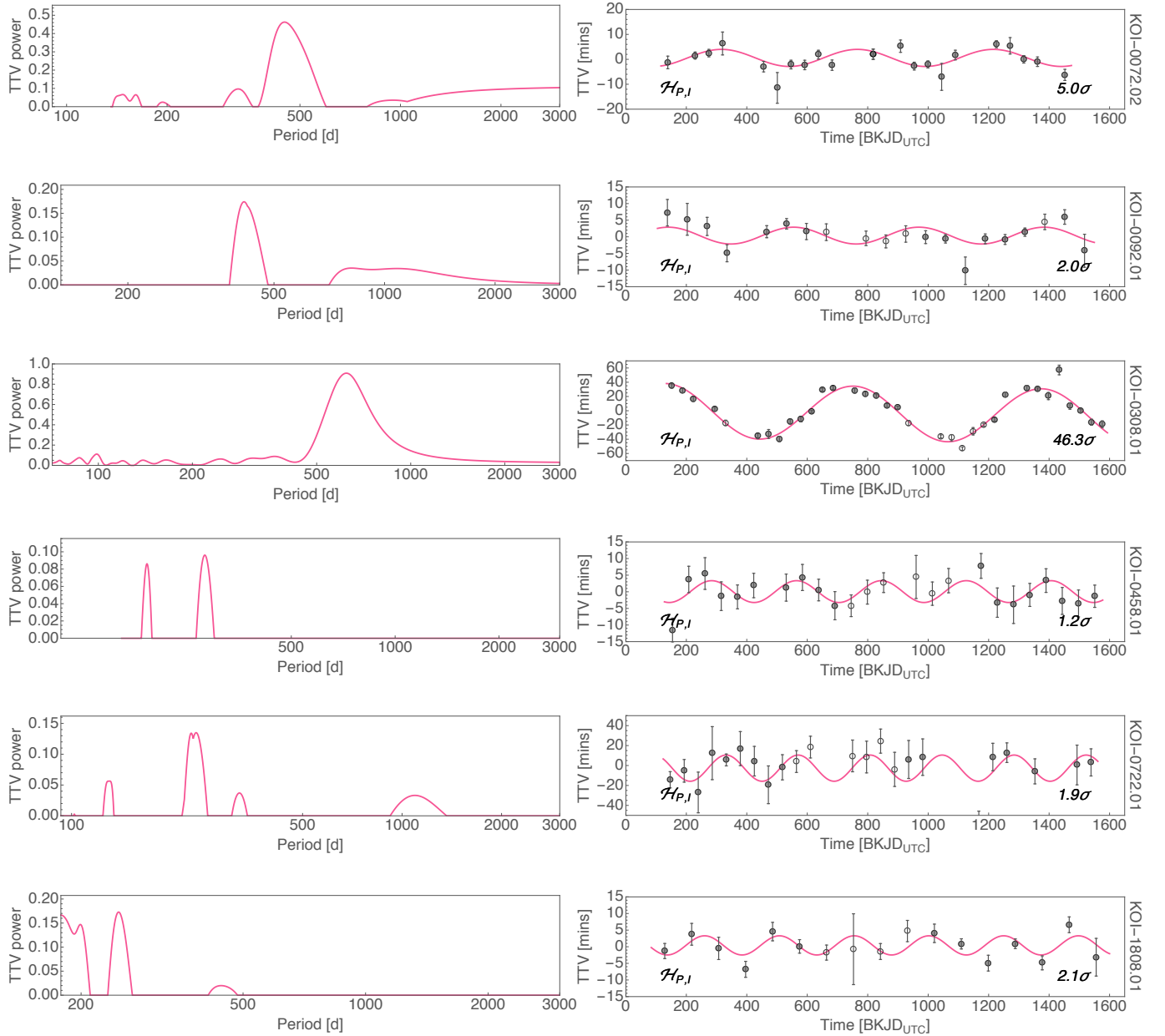


FIG. 5.— Right column shows the TTVs computed for 6 of the 12 KOIs which pass criteria B4a. These 6 KOIs have  $N \geq 17$  epochs and thus have too many free parameters for the global fit,  $\mathcal{H}_{P,TTV}$ , leading us to use a model of  $N$  independent fits,  $\mathcal{H}_{P,I}$ . The left panel shows the corresponding Lomb-Scargle periodogram with a BIC-based definition of power. The favored trial is plotted over the TTV data on the right panel, with the significance denoted in the corner.

incidental sample selection is highly improbable to be responsible. However, the sample studied by [Mazeh et al. \(2013\)](#) casts a much wider net than the carefully selected targets of TSA. Specifically, this rate is for the 2321 KOIs in the [Borucki et al. \(2011, 2012\)](#) catalogs with a  $\text{SNR} > 2.5$  (giving 1960 KOIs) exhibiting 7 or more transits in the first 12 quarters of data (giving 1897 KOIs). The latter filter excludes long period planets ( $P \lesssim 150$  days) and moreover the sample is heavily biased towards short period events due the higher detection probability ( $\sim P^{-5/3}$ ; [Gaudi 2006](#)).

The tension between these two rates could be resolved by a period dependency for the occurrence rate of de-

tectable TTVs. Our TSA sample is designed to pick gaseous planets in the habitable zone or further out, implying that habitable zone gaseous planets are frequently accompanied by additional planets, likely in period commensurabilities. These hidden planets probably reside in exterior orbits, in order to explain having not been seen to transit (since multi-planet systems are typically coplanar; [Fabrycky et al. 2014](#)). However, we caution that our TSA method uses a complex series of criteria, such as invoking tidal evolution models, which may make them not representative of habitable zone gaseous planets. The occurrence rate of dynamically active habitable zone or cooler gaseous planets is therefore an interesting

TABLE 4  
Planet properties as derived using model  $\mathcal{H}_P$ .

KOI	$p$	$\log_{10}(\rho_*$ [kg m <sup>-3</sup> ])	$b$	$P$ [d]	$\tau$ [BJKD]	$q_1$	$q_2$
KOI-0438.02	0.03147 <sup>+0.00128</sup> <sub>-0.00089</sub>	4.158 <sup>+0.086</sup> <sub>-0.295</sub>	0.36 <sup>+0.31</sup> <sub>-0.25</sub>	52.661599 <sup>+0.000097</sup> <sub>-0.000097</sub>	868.12003 <sup>+0.00077</sup> <sub>-0.00081</sub>	0.30 <sup>+0.34</sup> <sub>-0.18</sub>	0.25 <sup>+0.36</sup> <sub>-0.18</sub>
KOI-0518.03	0.03415 <sup>+0.00229</sup> <sub>-0.00088</sub>	3.44 <sup>+0.10</sup> <sub>-0.39</sub>	0.40 <sup>+0.33</sup> <sub>-0.28</sub>	247.3545 <sup>+0.0012</sup> <sub>-0.0013</sub>	858.8682 <sup>+0.0017</sup> <sub>-0.0017</sub>	0.48 <sup>+0.31</sup> <sub>-0.23</sub>	0.23 <sup>+0.31</sup> <sub>-0.15</sub>
KOI-0854.01	0.0398 <sup>+0.0020</sup> <sub>-0.0016</sub>	3.63 <sup>+0.14</sup> <sub>-0.40</sub>	0.46 <sup>+0.31</sup> <sub>-0.32</sub>	56.05608 <sup>+0.00021</sup> <sub>-0.00020</sub>	873.8370 <sup>+0.0020</sup> <sub>-0.0018</sub>	0.27 <sup>+0.37</sup> <sub>-0.19</sub>	0.31 <sup>+0.38</sup> <sub>-0.22</sub>
KOI-0868.01†	0.1516 <sup>+0.0024</sup> <sub>-0.0014</sub>	3.270 <sup>+0.019</sup> <sub>-0.014</sub>	0.816 <sup>+0.012</sup> <sub>-0.019</sub>	235.99726 <sup>+0.00013</sup> <sub>-0.00013</sub>	680.40440 <sup>+0.00023</sup> <sub>-0.00023</sub>	0.35 <sup>+0.30</sup> <sub>-0.17</sub>	0.28 <sup>+0.36</sup> <sub>-0.20</sub>
KOI-1361.01	0.03488 <sup>+0.00186</sup> <sub>-0.00088</sub>	3.626 <sup>+0.085</sup> <sub>-0.284</sub>	0.37 <sup>+0.30</sup> <sub>-0.25</sub>	59.87792 <sup>+0.00012</sup> <sub>-0.00013</sub>	869.7208 <sup>+0.0011</sup> <sub>-0.0011</sub>	0.52 <sup>+0.29</sup> <sub>-0.22</sub>	0.28 <sup>+0.30</sup> <sub>-0.17</sub>
KOI-1431.01†	0.0774 <sup>+0.0026</sup> <sub>-0.0014</sub>	3.254 <sup>+0.033</sup> <sub>-0.032</sub>	0.863 <sup>+0.010</sup> <sub>-0.011</sub>	345.15902 <sup>+0.00035</sup> <sub>-0.00035</sub>	633.46686 <sup>+0.00042</sup> <sub>-0.00043</sub>	0.52 <sup>+0.17</sup> <sub>-0.12</sub>	0.29 <sup>+0.38</sup> <sub>-0.21</sub>
KOI-1783.02†	0.0428 <sup>+0.0019</sup> <sub>-0.0040</sub>	3.12 <sup>+0.52</sup> <sub>-0.17</sub>	0.844 <sup>+0.044</sup> <sub>-0.285</sub>	294.0729 <sup>+0.0015</sup> <sub>-0.0014</sub>	768.9686 <sup>+0.0018</sup> <sub>-0.0018</sub>	0.39 <sup>+0.36</sup> <sub>-0.20</sub>	0.31 <sup>+0.40</sup> <sub>-0.21</sub>
KOI-1830.02	0.0440 <sup>+0.0031</sup> <sub>-0.0019</sub>	3.26 <sup>+0.18</sup> <sub>-0.27</sub>	0.52 <sup>+0.21</sup> <sub>-0.33</sub>	198.71078 <sup>+0.00058</sup> <sub>-0.00060</sub>	752.6515 <sup>+0.0016</sup> <sub>-0.0015</sub>	0.42 <sup>+0.25</sup> <sub>-0.14</sub>	0.55 <sup>+0.29</sup> <sub>-0.27</sub>
KOI-1876.01	0.0401 <sup>+0.0021</sup> <sub>-0.0013</sub>	3.757 <sup>+0.086</sup> <sub>-0.239</sub>	0.36 <sup>+0.27</sup> <sub>-0.25</sub>	82.53428 <sup>+0.00027</sup> <sub>-0.00027</sub>	869.4001 <sup>+0.0013</sup> <sub>-0.0013</sub>	0.40 <sup>+0.29</sup> <sub>-0.17</sub>	0.60 <sup>+0.27</sup> <sub>-0.28</sub>
KOI-2020.01	0.0370 <sup>+0.0039</sup> <sub>-0.0034</sub>	2.25 <sup>+0.39</sup> <sub>-0.40</sub>	0.71 <sup>+0.15</sup> <sub>-0.43</sub>	110.9650 <sup>+0.0011</sup> <sub>-0.0011</sub>	852.8362 <sup>+0.0045</sup> <sub>-0.0043</sub>	0.62 <sup>+0.25</sup> <sub>-0.24</sub>	0.43 <sup>+0.31</sup> <sub>-0.26</sub>
KOI-2686.01†	0.04053 <sup>+0.00113</sup> <sub>-0.00066</sub>	3.804 <sup>+0.054</sup> <sub>-0.145</sub>	0.30 <sup>+0.22</sup> <sub>-0.20</sub>	211.03338 <sup>+0.00051</sup> <sub>-0.00055</sub>	912.2156 <sup>+0.0012</sup> <sub>-0.0012</sub>	0.39 <sup>+0.25</sup> <sub>-0.15</sub>	0.44 <sup>+0.28</sup> <sub>-0.21</sub>
KOI-2691.01†	0.04262 <sup>+0.00156</sup> <sub>-0.00091</sub>	3.400 <sup>+0.070</sup> <sub>-0.196</sub>	0.33 <sup>+0.26</sup> <sub>-0.22</sub>	97.44645 <sup>+0.00028</sup> <sub>-0.00028</sub>	886.9525 <sup>+0.0012</sup> <sub>-0.0012</sub>	0.28 <sup>+0.21</sup> <sub>-0.11</sub>	0.65 <sup>+0.24</sup> <sub>-0.30</sub>
KOI-3263.01	0.48 <sup>+0.37</sup> <sub>-0.29</sub>	4.324 <sup>+0.064</sup> <sub>-0.055</sub>	1.28 <sup>+0.39</sup> <sub>-0.37</sub>	76.879333 <sup>+0.00046</sup> <sub>-0.00046</sub>	761.91724 <sup>+0.00025</sup> <sub>-0.00025</sub>	0.27 <sup>+0.37</sup> <sub>-0.20</sub>	0.46 <sup>+0.36</sup> <sub>-0.32</sub>
KOI-4005.01	0.02757 <sup>+0.00098</sup> <sub>-0.00093</sub>	3.14 <sup>+0.10</sup> <sub>-0.29</sub>	0.39 <sup>+0.29</sup> <sub>-0.26</sub>	178.1388 <sup>+0.0015</sup> <sub>-0.0013</sub>	744.5337 <sup>+0.00035</sup> <sub>-0.0035</sub>	0.14 <sup>+0.24</sup> <sub>-0.10</sub>	0.40 <sup>+0.38</sup> <sub>-0.29</sub>
KOI-4036.01	0.0244 <sup>+0.0106</sup> <sub>-0.0023</sub>	3.38 <sup>+0.29</sup> <sub>-1.50</sub>	0.62 <sup>+0.46</sup> <sub>-0.42</sub>	168.8102 <sup>+0.0015</sup> <sub>-0.0013</sub>	886.6796 <sup>+0.0040</sup> <sub>-0.0037</sub>	0.66 <sup>+0.23</sup> <sub>-0.31</sub>	0.59 <sup>+0.27</sup> <sub>-0.34</sub>
KOI-4054.01	0.02439 <sup>+0.00094</sup> <sub>-0.00084</sub>	3.28 <sup>+0.10</sup> <sub>-0.32</sub>	0.39 <sup>+0.31</sup> <sub>-0.27</sub>	169.1330 <sup>+0.0013</sup> <sub>-0.0011</sub>	878.3472 <sup>+0.0029</sup> <sub>-0.0035</sub>	0.19 <sup>+0.29</sup> <sub>-0.13</sub>	0.33 <sup>+0.40</sup> <sub>-0.24</sub>
KOI-0092.01	0.0249 <sup>+0.0017</sup> <sub>-0.0018</sub>	3.80 <sup>+0.38</sup> <sub>-0.30</sub>	0.71 <sup>+0.12</sup> <sub>-0.42</sub>	65.704565 <sup>+0.00052</sup> <sub>-0.00054</sub>	794.48803 <sup>+0.00032</sup> <sub>-0.00032</sub>	0.52 <sup>+0.32</sup> <sub>-0.16</sub>	0.17 <sup>+0.31</sup> <sub>-0.11</sub>
KOI-0112.01	0.0282 <sup>+0.0010</sup> <sub>-0.0015</sub>	2.65 <sup>+0.29</sup> <sub>-0.13</sub>	0.784 <sup>+0.045</sup> <sub>-0.164</sub>	51.079310 <sup>+0.00061</sup> <sub>-0.00061</sub>	900.29048 <sup>+0.00057</sup> <sub>-0.00057</sub>	0.338 <sup>+0.125</sup> <sub>-0.071</sub>	0.38 <sup>+0.38</sup> <sub>-0.27</sub>
KOI-0209.01	0.07158 <sup>+0.00040</sup> <sub>-0.00035</sub>	2.584 <sup>+0.024</sup> <sub>-0.026</sub>	0.233 <sup>+0.073</sup> <sub>-0.106</sub>	50.790364 <sup>+0.00021</sup> <sub>-0.00021</sub>	846.69768 <sup>+0.00019</sup> <sub>-0.00019</sub>	0.232 <sup>+0.036</sup> <sub>-0.034</sub>	0.458 <sup>+0.081</sup> <sub>-0.066</sub>
KOI-0276.01	0.01933 <sup>+0.00089</sup> <sub>-0.00050</sub>	3.39 <sup>+0.16</sup> <sub>-0.27</sub>	0.50 <sup>+0.21</sup> <sub>-0.32</sub>	41.745992 <sup>+0.00034</sup> <sub>-0.00033</sub>	961.82689 <sup>+0.00036</sup> <sub>-0.00037</sub>	0.44 <sup>+0.19</sup> <sub>-0.12</sub>	0.16 <sup>+0.19</sup> <sub>-0.11</sub>
KOI-0308.01*	0.02365 <sup>+0.0020</sup> <sub>-0.00020</sub>	2.477 <sup>+0.036</sup> <sub>-0.036</sub>	0.892 <sup>+0.17</sup> <sub>-0.17</sub>	35.597254 <sup>+0.00043</sup> <sub>-0.00044</sub>	899.47632 <sup>+0.00057</sup> <sub>-0.00056</sub>	-	-
KOI-0374.01	0.0249 <sup>+0.0013</sup> <sub>-0.0011</sub>	2.72 <sup>+0.25</sup> <sub>-0.27</sub>	0.61 <sup>+0.16</sup> <sub>-0.36</sub>	172.70406 <sup>+0.00049</sup> <sub>-0.00051</sub>	755.0368 <sup>+0.0013</sup> <sub>-0.0013</sub>	0.45 <sup>+0.20</sup> <sub>-0.12</sub>	0.24 <sup>+0.26</sup> <sub>-0.15</sub>
KOI-0398.01	0.0945 <sup>+0.0020</sup> <sub>-0.0018</sub>	3.461 <sup>+0.049</sup> <sub>-0.045</sub>	0.616 <sup>+0.039</sup> <sub>-0.050</sub>	51.846858 <sup>+0.00028</sup> <sub>-0.00028</sub>	844.09103 <sup>+0.00022</sup> <sub>-0.00022</sub>	0.75 <sup>+0.17</sup> <sub>-0.21</sub>	0.330 <sup>+0.166</sup> <sub>-0.093</sub>
KOI-0458.01	0.25 <sup>+0.52</sup> <sub>-0.18</sub>	2.70 <sup>+0.23</sup> <sub>-0.12</sub>	1.18 <sup>+0.54</sup> <sub>-0.24</sub>	53.718027 <sup>+0.00067</sup> <sub>-0.00068</sub>	906.41442 <sup>+0.00062</sup> <sub>-0.00062</sub>	0.25 <sup>+0.37</sup> <sub>-0.19</sub>	0.57 <sup>+0.33</sup> <sub>-0.38</sub>
KOI-0847.01	0.0568 <sup>+0.0023</sup> <sub>-0.0014</sub>	2.664 <sup>+0.099</sup> <sub>-0.155</sub>	0.41 <sup>+0.19</sup> <sub>-0.27</sub>	80.87199 <sup>+0.00015</sup> <sub>-0.00015</sub>	850.87236 <sup>+0.00087</sup> <sub>-0.00088</sub>	0.41 <sup>+0.21</sup> <sub>-0.14</sub>	0.42 <sup>+0.27</sup> <sub>-0.17</sub>
KOI-1535.01	0.01844 <sup>+0.00055</sup> <sub>-0.00055</sub>	3.24 <sup>+0.10</sup> <sub>-0.58</sub>	0.40 <sup>+0.26</sup> <sub>-0.28</sub>	70.69782 <sup>+0.00026</sup> <sub>-0.00025</sub>	824.8510 <sup>+0.0016</sup> <sub>-0.0019</sub>	0.22 <sup>+0.30</sup> <sub>-0.15</sub>	0.20 <sup>+0.39</sup> <sub>-0.16</sub>
KOI-1726.01	0.02632 <sup>+0.00213</sup> <sub>-0.00082</sub>	3.38 <sup>+0.13</sup> <sub>-0.35</sub>	0.45 <sup>+0.28</sup> <sub>-0.30</sub>	44.964066 <sup>+0.00056</sup> <sub>-0.00055</sub>	819.02111 <sup>+0.00061</sup> <sub>-0.00060</sub>	0.44 <sup>+0.26</sup> <sub>-0.17</sub>	0.49 <sup>+0.31</sup> <sub>-0.24</sub>
KOI-1808.01	0.02816 <sup>+0.00296</sup> <sub>-0.00095</sub>	3.88 <sup>+0.18</sup> <sub>-0.63</sub>	0.52 <sup>+0.34</sup> <sub>-0.36</sub>	89.193549 <sup>+0.00078</sup> <sub>-0.00080</sub>	931.37212 <sup>+0.00047</sup> <sub>-0.00048</sub>	0.39 <sup>+0.33</sup> <sub>-0.16</sub>	0.21 <sup>+0.36</sup> <sub>-0.14</sub>
KOI-1871.01	0.0312 <sup>+0.0026</sup> <sub>-0.0012</sub>	3.440 <sup>+0.086</sup> <sub>-0.264</sub>	0.36 <sup>+0.29</sup> <sub>-0.25</sub>	92.72967 <sup>+0.00035</sup> <sub>-0.00033</sub>	826.5496 <sup>+0.0018</sup> <sub>-0.0020</sub>	0.57 <sup>+0.25</sup> <sub>-0.20</sub>	0.68 <sup>+0.21</sup> <sub>-0.23</sub>
KOI-2065.01	0.041 <sup>+0.020</sup> <sub>-0.013</sub>	2.67 <sup>+1.26</sup> <sub>-0.32</sub>	0.942 <sup>+0.045</sup> <sub>-0.620</sub>	80.23201 <sup>+0.00053</sup> <sub>-0.00049</sub>	1044.9485 <sup>+0.0027</sup> <sub>-0.0026</sub>	0.73 <sup>+0.20</sup> <sub>-0.34</sub>	0.65 <sup>+0.25</sup> <sub>-0.39</sub>
KOI-2762.01	0.0345 <sup>+0.0021</sup> <sub>-0.0014</sub>	3.45 <sup>+0.12</sup> <sub>-0.44</sub>	0.41 <sup>+0.36</sup> <sub>-0.29</sub>	132.99679 <sup>+0.00099</sup> <sub>-0.00090</sub>	923.3727 <sup>+0.0030</sup> <sub>-0.0031</sub>	0.33 <sup>+0.37</sup> <sub>-0.23</sub>	0.29 <sup>+0.37</sup> <sub>-0.21</sub>
KOI-5284.01	0.28 <sup>+0.49</sup> <sub>-0.23</sub>	3.30 <sup>+1.12</sup> <sub>-0.15</sub>	1.21 <sup>+0.50</sup> <sub>-0.68</sub>	389.3128 <sup>+0.0023</sup> <sub>-0.0022</sub>	1129.9934 <sup>+0.0018</sup> <sub>-0.0019</sub>	0.56 <sup>+0.30</sup> <sub>-0.39</sub>	0.63 <sup>+0.27</sup> <sub>-0.43</sub>
KOI-0072.02*	0.020414 <sup>+0.00062</sup> <sub>-0.00062</sub>	3.0286 <sup>+0.0016</sup> <sub>-0.0016</sub>	0.3182 <sup>+0.0063</sup> <sub>-0.0063</sub>	45.294314 <sup>+0.00032</sup> <sub>-0.00031</sub>	908.68114 <sup>+0.00028</sup> <sub>-0.00027</sub>	-	-
KOI-0245.01	0.023201 <sup>+0.00062</sup> <sub>-0.00059</sub>	5.088 <sup>+0.012</sup> <sub>-0.012</sub>	0.5350 <sup>+0.0084</sup> <sub>-0.0086</sub>	39.792238 <sup>+0.00011</sup> <sub>-0.00011</sub>	772.133411 <sup>+0.000100</sup> <sub>-0.000099</sub>	0.382 <sup>+0.030</sup> <sub>-0.028</sub>	0.436 <sup>+0.057</sup> <sub>-0.056</sub>
KOI-0386.02	0.0265 <sup>+0.0026</sup> <sub>-0.0011</sub>	3.21 <sup>+0.19</sup> <sub>-0.59</sub>	0.53 <sup>+0.32</sup> <sub>-0.36</sub>	76.73312 <sup>+0.00035</sup> <sub>-0.00034</sub>	891.2658 <sup>+0.0019</sup> <sub>-0.0019</sub>	0.38 <sup>+0.33</sup> <sub>-0.21</sub>	0.30 <sup>+0.39</sup> <sub>-0.21</sub>
KOI-0518.02	0.02342 <sup>+0.00135</sup> <sub>-0.00080</sub>	3.32 <sup>+0.14</sup> <sub>-0.44</sub>	0.47 <sup>+0.31</sup> <sub>-0.32</sub>	44.00035 <sup>+0.00012</sup> <sub>-0.00013</sub>	870.7686 <sup>+0.0014</sup> <sub>-0.0015</sub>	0.27 <sup>+0.30</sup> <sub>-0.16</sub>	0.30 <sup>+0.40</sup> <sub>-0.22</sub>
KOI-0722.01	0.02070 <sup>+0.00105</sup> <sub>-0.00056</sub>	2.95 <sup>+0.13</sup> <sub>-0.45</sub>	0.45 <sup>+0.33</sup> <sub>-0.31</sub>	46.40648 <sup>+0.00015</sup> <sub>-0.00015</sub>	192.9939 <sup>+0.0021</sup> <sub>-0.0022</sub>	0.21 <sup>+0.22</sup> <sub>-0.12</sub>	0.29 <sup>+0.40</sup> <sub>-0.22</sub>
KOI-1783.01	0.0761 <sup>+0.0045</sup> <sub>-0.0035</sub>	2.972 <sup>+0.085</sup> <sub>-0.051</sub>	0.916 <sup>+0.015</sup> <sub>-0.025</sub>	134.47864 <sup>+0.00013</sup> <sub>-0.00013</sub>	841.67398 <sup>+0.00038</sup> <sub>-0.00040</sub>	0.62 <sup>+0.29</sup> <sub>-0.35</sub>	0.48 <sup>+0.37</sup> <sub>-0.34</sub>
KOI-2358.01	0.01955 <sup>+0.00241</sup> <sub>-0.00078</sub>	2.68 <sup>+0.15</sup> <sub>-0.64</sub>	0.47 <sup>+0.38</sup> <sub>-0.32</sub>	56.49384 <sup>+0.00034</sup> <sub>-0.00034</sub>	991.3899 <sup>+0.00037</sup> <sub>-0.00033</sub>	0.54 <sup>+0.30</sup> <sub>-0.27</sub>	0.31 <sup>+0.34</sup> <sub>-0.21</sub>
KOI-3663.01	0.09099 <sup>+0.00046</sup> <sub>-0.00051</sub>	3.347 <sup>+0.019</sup> <sub>-0.017</sub>	0.276 <sup>+0.045</sup> <sub>-0.062</sub>	282.525517 <sup>+0.00093</sup> <sub>-0.00094</sub>	928.12271 <sup>+0.00013</sup> <sub>-0.00013</sub>	0.426 <sup>+0.049</sup> <sub>-0.043</sub>	0.316 <sup>+0.037</sup> <sub>-0.033</sub>
KOI-3681.01	0.08942 <sup>+0.00013</sup> <sub>-0.00013</sub>	2.3654 <sup>+0.0058</sup> <sub>-0.0056</sub>	0.215 <sup>+0.020</sup> <sub>-0.023</sub>	217.831780 <sup>+0.00050</sup> <sub>-0.00050</sub>	892.315527 <sup>+0.00096</sup> <sub>-0.000100</sub>	0.279 <sup>+0.012</sup> <sub>-0.012</sub>	0.381 <sup>+0.017</sup> <sub>-0.016</sub>

†:  $\mathcal{H}_{P,TTV}$  used instead due to significant TTVs present

\*:  $\mathcal{H}_{P,I}$  used instead due to significant TTVs present and  $\geq 17$  transit epochs

question to pursue in future work.

#### 5.4. Empirical Sensitivity to Exomoons

Several previous works have attempted to estimate the expected sensitivity of *Kepler* and other telescopes to exomoons (e.g. Kipping et al. 2009; Simon et al. 2009). None of these works have gauged the sensitivity of full photodynamics, rather focusing on just one or two of the multitude of effects by which an exomoon may betray its presence. Further, real noise structure and complex inter-parameter degeneracies have not been realistically modeled. The most robust estimate of our photometric sensitivity to exomoons comes from examining the empirical upper limits derived from a reasonably large sample, such as those from the HEK project surveys.

Of the 57 unique KOIs studied, we find 46 null detections which are suitable for deriving upper limits from. This indicates that we obtain null detections for  $(81 \pm 5)\%$  of cases studied, with the others being false-positives. From the null detections, we find a diverse range of sensitivities in  $(M_S/M_P)$ , ranging from  $1.9 \times 10^{-3}$  (95.45% upper limit of KOI-2020.01) to nearly unity, as shown in Figure 7 (for reference, the Earth-Moon mass-ratio is  $12.3 \times 10^{-3}$ ). This diversity is likely due to a complex combination of factors, such as the target magnitude, planetary transit depth and duration, correlated noise structure, Hill sphere size, latent TTVs from perturbing planets, photometric cadence and number of transits. Regardless, we are able to infer that, assuming our sample is typical, the null detections are sensitive to Earth-

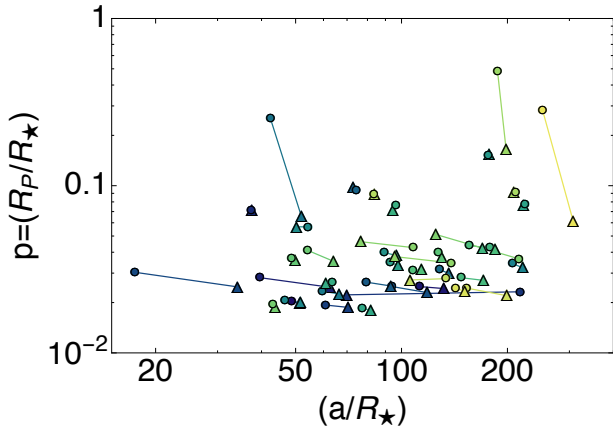


FIG. 6.— Comparison of the NASA Exoplanet Archive listed transit parameters (triangles) versus the values derived in this work (circles). Specific KOIs are connected by a line and have the same color coding. The plotted points represent the medians of the parameter posteriors.

Moon mass-ratios or better for  $\simeq 15\%$  of cases and to Pluto-Charon mass-ratios for  $\simeq 47\%$  (based on 95.45% confidences).

The relative mass limits of  $(M_S/M_P)$  may be converted to absolute masses limits in  $M_S$  by estimating  $M_P$ . For cases such as Kepler-10c, the physical mass is known (Dumusque et al. 2014), and here our upper limit corresponds to 1.7 Ganymede masses (at 95.45% confidence), demonstrating our ability to find moons akin to those in the Solar System. In the other cases, we must assign a mass based on the observed radius,  $R_P$ . For self-consistency, we use the same  $R_P$ - $M_P$  relation used for TSA, namely that discussed in Kipping et al. (2014a), which is predominantly an empirical relationship. As shown in the right panel of Figure 7, this allows to estimate that we are sensitive to Earth-like moons or smaller for  $\simeq 40\%$  of the null cases. The lowest mass exomoon that can be considered capable of supporting an Earth-like atmosphere is thought to be at  $0.3 M_\oplus$  (Raymond et al. 2007), for which we find sensitivity for  $\simeq 30\%$  of null cases.

In summary then, based on empirical sensitivity limits, we show for the first time that the HEK project is sensitive to even the smallest moons capable of being Earth-like for 1 in 4 cases (after accounting for false-positives). In terms of planet-mass ratios, we find even that the Earth-Moon mass-ratio is detectable for 1 in 8 of cases, posing a challenge but not an insurmountable barrier. Mass ratios of  $\sim 10^{-4}$ , such as that of the Galilean satellites, have never been achieved. However, if Galilean-like satellites reside around lower-mass planets than Jupiter, of order  $\sim 20 M_\oplus$ , then we do find sensitivity, as demonstrated by the limit of 1.7 Ganymede masses achieved for Kepler-10c.

### 5.5. Computational Demands

We briefly discuss the computational demands of the HEK survey to date. Previous surveys generally used less than the full *Kepler* time series (Q0-Q17) due to the timeline of the data releases. In contrast, all 41 KOIs surveyed here used all available quarters, providing a fairer assessment of computational requirements for future surveys. We recorded the computational time used for each

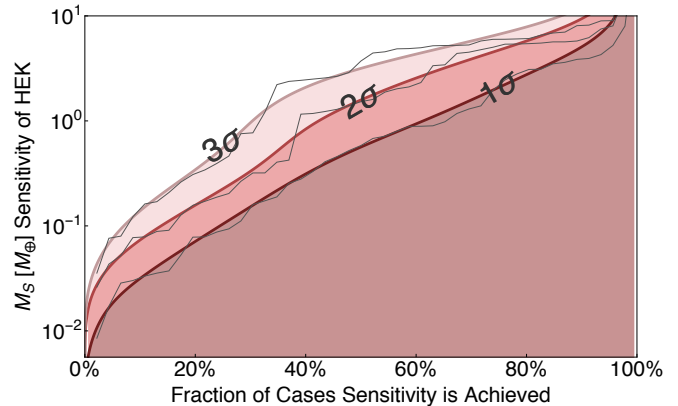
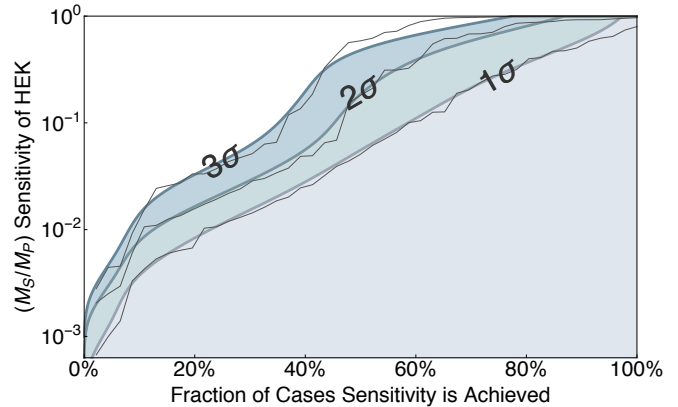


FIG. 7.— **Upper:** Smoothed empirical sensitivity of the HEK survey to the satellite-to-planet mass-ratio. Based on 46 null results (thin gray line) drawn from the 57 unique KOIs studied. HEK is sensitive to Earth-Moon mass-ratios for  $\simeq 15\%$  of null cases and to Pluto-Charon mass-ratios for  $\simeq 47\%$  (based on 95.45% confidences). **Lower:** Same as top, except sensitivity quoted in absolute masses via estimated planetary masses. HEK is sensitive to  $0.3 M_\oplus$  mini-Earths for  $\simeq 30\%$  of cases and to Earths for  $\simeq 40\%$  (based on 95.45% confidences).

model fit  $\mathcal{H}_S$ , in order to better understand our requirements. A histogram of the CPU times is shown in Figure 8, with a mean time of 33,000 hours per KOI. Note that these times do not include the planet-only fits (negligible times) and TTV fits (sizable but less demanding). For all fits, the fits were conducted on AMD Opteron 62xx/63xx CPUs. The spread in times appears mostly linked to the number of transit epochs fitted, with larger time series naturally requiring more overhead. With current in-house server capacity, we estimate that we are able to survey at least 100 KOIs per year.

### 5.6. The Effects of Correlated Noise

Despite the groundbreaking precision achieved by *Kepler* (Christiansen et al. 2012), when one seeks low signal-to-noise events then the effects of time-correlated noise become important. This is particularly salient for exomoons, since the transits do not follow a simple ephemeris which can be used to check for repeatability (Kipping 2011). This allows the model great flexibility in explaining any slight random changes in flux, leading to spurious detections (e.g. Kipping et al. 2015).

One strategy to guard against correlated noise is to use a likelihood function more suited for such structure,

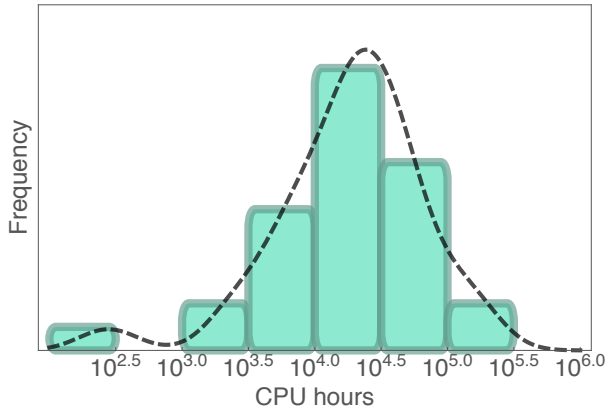


FIG. 8.— Histogram of the number of CPU hours used for model  $\mathcal{H}_S$  of the 41 KOIs surveyed in this work. The distribution has a mode of 24,000 CPU hours and a mean of 33,000 CPU hours.

for example using wavelets or Gaussian processes (pedagogical examples of these methods applied to photometry can be found in [Carter & Winn 2009](#) and [Gibson et al. 2012](#), respectively). However, these methods have so much flexibility that they may fit-out the very low amplitude signals we seek. An alternative strategy, as employed in this work, is to use vetting criteria, such as the double likelihood test F2 and insights from our photodynamical fits. Whilst maintaining the use of a Gaussian likelihood leads to more false-positives, it at least allows us see the full array of candidate signals and to assess them accordingly. Since the use of Gaussian likelihood functions is so prevalent within the community, we here discuss the rate of false-positives induced by correlated noise structure.

Correlated noise directly affects the time series photometry, potentially mimicking transit-like signals and leading to spurious detections of  $(R_S/R_P)$ . Whilst correlated noise can also affect the TTVs by distorting the planetary transit profile ([Mazeh et al. 2015](#)), such transit distortions are usually fitted out by the radius effect of our moon model, as seen in the example of Figure 9. In what follows, we focus on the effect of correlated noise on moon transit signals, i.e. parameter  $(R_S/R_P)$ . In our survey, a non-zero  $(R_S/R_P)$  moon fit can be caused by two distinct reasons:

- A] The latent prior of  $\rho_S < 27.9 \text{ g cm}^{-3}$  (see §3) technically forbids  $(R_S/R_P) = 0$ , thereby forcing genuinely null  $(R_S/R_P)$  cases to be either positive or negative.
- B] Time correlated noise may drive the fits towards a false-positive likelihood minimum, since we adopt a Gaussian likelihood function.

It is of particular interest to understand how frequently case B occurs, which severely affects all methods seeking evidence of exomoons via their transits. In hindsight, not imposing the latent  $\rho_S$  prior would be the most effective way to measure the occurrence of spurious  $(R_S/R_P)$  detections due to correlated noise. However, we discuss here an alternative approach using the information in hand. The mean satellite density is computed using Equation 5 of [Kipping \(2010b\)](#):

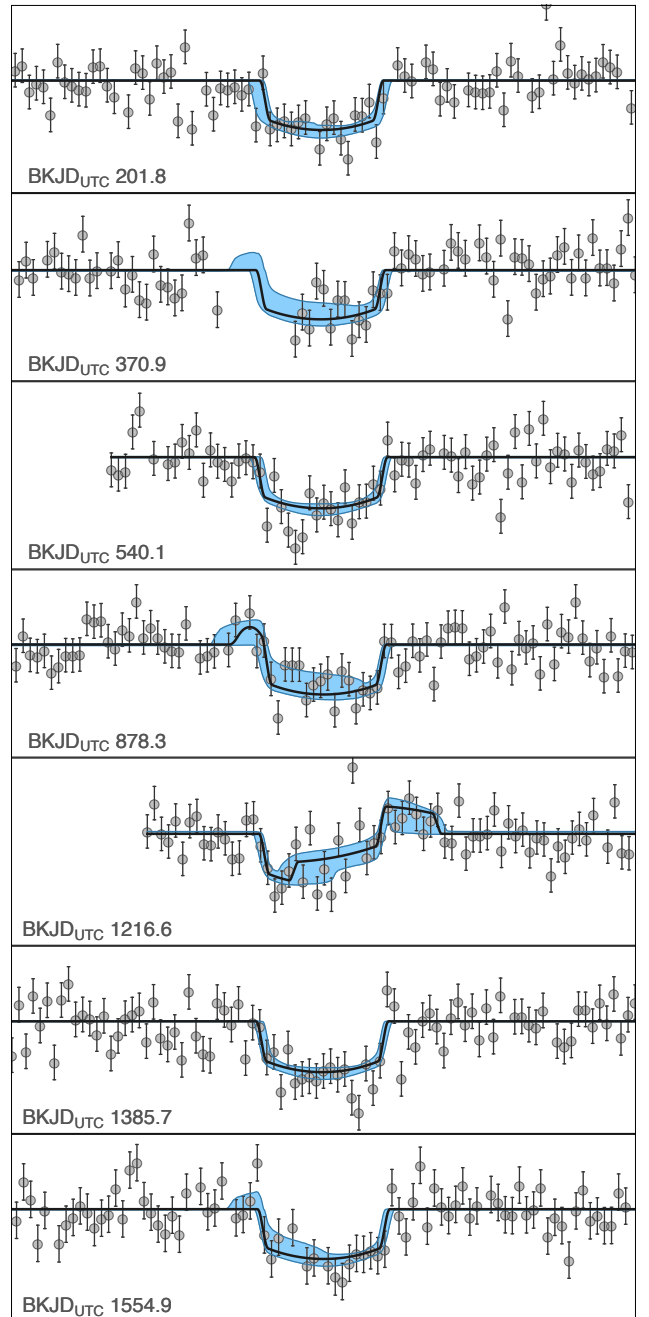


FIG. 9.— Example of a “negative radius” (inverted transits) exomoon solution, which occurs for around half of all KOIs surveyed. The transit light curves used for fitting KOI-4054.01 are shown, along with the maximum a-posteriori realization of our planet+moon model (black line) and the 95.45% credible intervals (blue shaded region). This model is favored over a planet-only at  $3.5 \sigma$  with  $(R_S/R_P) = -0.71 \pm 0.09$ , driven by correlated noise.

$$\rho_S = \rho_P \frac{(M_S/M_P)}{|R_S/R_P|^3}. \quad (1)$$

Since we impose the condition that  $\rho_S < 27.9 \text{ g cm}^{-3}$ , then plotting the joint posterior of  $(\rho_P(M_S/M_P))$  and  $|R_S/R_P|^3$  will have an excluded region defined by a straight line passing through the origin of gradient



27.9 g cm<sup>-3</sup>. We inspected each of the joint posteriors as described, identifying cases where the posterior was bunched up against this boundary, indicating the latent prior was likely driving a non-zero ( $R_S/R_P$ ) solution (i.e. case A). Of the 41 KOIs surveyed, we find that 22 show no evidence for being affected by the latent  $\rho_S$  prior and therefore the non-zero ( $R_S/R_P$ ) solution is reasoned, by deduction, to be caused by time correlated noise.

This estimate provides a handle as to the prevalence of correlated noise-induced spurious moon-like transits, indicating that  $(54 \pm 8)\%$  of KOIs surveyed are affected. In future work, we intend to relax the latent priors and conduct a more in-depth analysis of this question. Of the 22 identified cases, 8 yield negative radius moon solutions, compatible with the expectation of  $11 \pm 2.3$ , assuming that correlated noise induces negative radius transits with a  $p$ -value of 0.5.

If we had sought evidence for exomoons by seeking exomoon radius signals alone, and had not used a time-correlated noise likelihood, we would have erroneously inferred evidence for exomoons in around half of these cases, which is over one quarter ( $\sim 26\%$ ) of all KOIs surveyed. Thanks to photodynamics and our vetting criteria we were able to identify these spurious cases.

Although our survey strategy is robust against these time-correlated noise-induced moon-like transits, other exomoon search methods that do not use photodynamics may struggle to identify these frequent occurrences.

We highlight these cases as a service to the community, to emphasize that exomoons live in the regime where correlated noise is present and one must employ methods to guard against it when seeking such signals.

#### ACKNOWLEDGEMENTS

This work made use of the Michael Dodds Computing Facility, for which we are grateful to Michael Dodds, Carl Allegritti, David Van Buren, Anthony Grange, Cameron Lehman, Ivan Longland, Dell Lunceford, Gregor Rothfuss, Matt Salzberg, Richard Sundvall, Graham Symmonds, Kenneth Takigawa, Marion Adam, Dour High Arch, Mike Barrett, Greg Cole, Sheena Dean, Steven Delong, Robert Goodman, Mark Greene, Stephen Kitt, Robert Leyland, Matthias Meier, Roy Mitsuoka, David Nicholson, Nicole Papas, Steven Purcell, Austen Redman, Michael Sheldon, Ronald Sonenthal, Nicholas Steinbrecher, Corbin Sydney, John Vajgrt, Louise Valmorira, Hunter Williams, Troy Winarski and Nigel Wright. DMK and DN acknowledge partial support from NASA grant NNX15AF09G. JH and GB acknowledge partial support from NASA grant NNX13AJ15G. JH acknowledges support from NNX14AF87G. DN acknowledges support from NSF AST-1008890. This paper includes data collected by the *Kepler* mission. Funding for the *Kepler* mission is provided by the NASA Science Mission directorate.

#### REFERENCES

- Ballard, S., Charbonneau, D., Fressin, F., et al. 2013, ApJ, 773, 98  
 Barclay, T., Rowe, J. F., Lissauer, J. J., et al. 2013, Nature, 494, 452  
 Barnes, J. W. & O'Brien, D. P. 2002, ApJ, 575, 1087  
 Béky, B., Holman, M. J., Kipping, D. M. & Noyes, R. W. 2014, ApJ, 788, 1  
 Borucki, W. J., Koch, D. G., Basri, G., et al. 2011, ApJ, 736, 19  
 Borucki, W. J., Koch, D. G., Batalha, N., et al. 2012, ApJ, 745, 120  
 Carter, J. A. & Winn, J. N. 2009, ApJ, 704, 51  
 Christiansen, J. L., Jenkins, J. M., Caldwell, D. A., et al. 2012, PASP, 124, 1279  
 Claret, A. & Bloemen, S. 2011, A&A, 529, 75  
 Deck, K. M. & Agol, E. 2014, ApJ, submitted (arXiv:1411.0004)  
 Dumusque, X., Bonomo, A. S., Haywood, R. D., et al. 2014, ApJ, 789, 154  
 Fabrycky, D. C., Lissauer, J. J., Ragozzine, D., et al. 2014, ApJ, 790, 146  
 Feroz, F. & Hobson, M. P. 2008, MNRAS, 384, 449  
 Feroz, F., Hobson, M. P. & Bridges, M. 2009, MNRAS, 398, 1601  
 Feroz, F. 2013, "Proceedings 59th ISI World Statistics Congress", 25-30 August 2013, Hong Kong, p. 2081  
 Fewell, M. 2006, "Area of Common Overlap of Three Circles", Tech. Rep. DSTO-TN-0722 [http://hdl.handle.net/1947/4551]  
 Fischer, D. A., Schwamb, M. E., Schawinski, K., et al. 2012, MNRAS, 419, 2900  
 Gaudi, B. S. 2006, arXiv:astro-ph/0612141  
 Gibson, N. P., Aigrain, S., Roberts, S., et al. 2012, MNRAS, 419, 2683  
 Handley, W. J., Hobson, M. P. & Lasenby, A. N. 2015, MNRAS, submitted (arXiv:1502.01856)  
 Heller, R. 2014, ApJ, 787, 14  
 Huang, X., Bakos, G. A. & Hartman, J. D. 2013, MNRAS, 429, 2001  
 Kipping, D. M. 2009a, MNRAS, 392, 181  
 —. 2009b, MNRAS, 396, 1793  
 —. 2010a, MNRAS, 408, 1758  
 —. 2010b, MNRAS, 409, L119  
 —. 2011, MNRAS, 416, 689  
 —. 2013, MNRAS, 435, 2152  
 Kipping, D. M., Fossey, S. J. & Campanella, G. 2009, MNRAS, 400, 398  
 Kipping, D. M. & Tinetti, G. 2010, MNRAS, 407, 2589  
 Kipping, D. M., Bakos, G. Á., Buchhave, L., Nesvorný, D. & Schmitt, A. 2012, ApJ, 750, 115  
 Kipping, D. M., Hartman, J., Buchhave, L. A., et al. 2013a, ApJ, 770, 101  
 Kipping, D. M., Forgan, D., Hartman, J., et al. 2013b, ApJ, 777, 134  
 Kipping, D. M., Nesvorný, D., Buchhave, L. A., et al. 2014a, ApJ, 784, 28  
 Kipping, D. M., Torres, G., Buchhave, L. A., et al. 2014b, ApJ, 795, 25  
 Kipping, D. M., Huang, X., Nesvorný, D., et al. 2015, ApJ, 799, 14  
 Kundurthy, P., Agol, E., Becker, A. C., et al. 2011, ApJ, 731, 123  
 Lewis, K. 2014, STScI "Habitable Worlds Across Time and Space" meeting, oral presentation  
 Lucy, L. B. & Sweeney, M. A. 1971, 76, 544  
 Mandel, K. & Agol, E. 2002, ApJ, 580, 171  
 Mazeh, T., Nachmani, G., Holczer, T., et al. 2013, ApJS, 208, 16  
 Mazeh, T., Holczer, T. & Shporer, A. 2015, ApJ, 800, 142  
 Namouni, F. 2010, ApJ, 719, 145  
 Nesvorný, D., Kipping, D. M., Buchhave, L., et al. 2012, Science, 336, 1133  
 Nesvorný, D. & Vokrouhlický, D. 2014, ApJ, 790, 58  
 Raymond, S. N., Scalzo, J. & Meadows, V. S. 2007, ApJ, 669, 606  
 Rowe, J. F., Bryson, S. T., Marcy, G. W., et al. 2014, ApJ, 784, 45  
 Sartoretti, P. & Schneider, J. 1999, A&AS, 134, 553  
 Schwamb, M. E., Orosz, J. A., Carter, J. A., et al. 2013, ApJ, 768, 127  
 Simon, A. E., Szabó, Gy. M. & Szatmáry, K. 2009, EM&P, 105, 385  
 Simon, A. E., Szabó, Gy. M., Kiss, L. L. & Szatmáry, K. 2012, MNRAS, 419, 164  
 Skilling, J. 2004, in Fischer R., Preuss R., Toussaint U. V., eds, American Institute of Physics Conference Series Nested Sampling. pp 395405

- Smith, J. C., Stumpe, M. C., Van Cleve, J. E., et al. 2012, *PASP*, 124, 1000
- Stumpe, M. C., Smith, J. C., Van Cleve, J. E., et al. 2012, *PASP*, 124, 985
- Szabó, R., Szabó, Gy. M., Dály, G., et al. 2013, *A&A*, 553, 17
- Torres, G., Kipping, D. M., Fressin, F., et al. 2015, *ApJ*, 800, 99
- Wang, J., Fischer, D. A., Barclay, T., et al. 2013, *ApJ*, 776, 10
- Zsom, A., Seager, S., de Wit, J. & Stamenković, V. 2013, *ApJ*, 778, 109